Remarks

Claims 6-9, 11, 14, 16, 18-50, 54, 56-58, and 63-71 are pending in the application. Of these claims, claims 9, 11, 16, 18-50, 54, and 56-58 are withdrawn from consideration.

35 U.S.C. § 112, ¶2 (Indefiniteness)

Claim 53 is rejected under 35 U.S.C. § 112, second paragraph, as being indefinite by the use of the term "metal-rich." Claim 53 has been cancelled, and the term "metal-rich" has been added to independent claims 6-8 and claim 14.

The Office action finds,

> The phrase 'metal rich' renders the claim indefinite as it is unclear which metal is being considered. ... While the attached article is helpful for the term the coating has only one metal in the mental compound and thus it is clear which metal is being referred to but in the instant claim there are two metals claimed, rendering the claim indefinite.

Applicants respectfully traverse this rejection.

The relevant statute, 35 U.S.C. § 12 ¶ 2, requires that the claims "particularly [point] out and distinctly [claim] the subject matter which the applicant regards as his invention." The operative standard for determining whether this requirement has been met is "whether those skilled in the art would understand what is claimed when the claim is read in light of the specification."[1]

Applicants have explained to the Examiner, with the support of an article attached to the response of May 10, 2005, that the term "metal-rich" recited in claims of the present application is an established term known to those skilled in the art when the present application was filed. The term "metal-rich" means that the amount of metal(s) in a substance is more than what would be considered to be the normal stoichiometric amount. It is irrelevant whether the substance contains more than one metal or not. If there are two or more metals in a metal compound, a person of

[1] *Beachcombers, International Inc. v. WildeWood Creative Products Inc.*, 31 U.S.P.Q.2d 1653, 1656 (Fed. Cir. 1994).

ordinary skill in the art will still understand that the compound is "metal-rich" if the total amount of the two or more metals in the compound is more than the total amount of the metals in a corresponding normal stoichiometric compound.

To evidence that the term "metal-rich" is a well known adjective used by chemists and material scientists to generally describe a substance, even if it contains more than one metal, when the total amount of metals in the substance is more than what would be considered to be the normal stoichiometric amount, five exemplary articles are attached in Exhibits A-E. All five articles were published before the present application was filed. Exhibit A is a 1976 article, in which the author studied stoichiometric mawsonite, $Cu_6Fe_2SnS_8$ and "two metal-rich copper-iron sulfides, haycockite, $Cu_4Fe_5S_8$, and mooihoekite, $Cu_9Fe_9S_{16}$." Exhibit A, page 529. The author does not specify which one of the two metals is rich when referring to $Cu_4Fe_5S_8$ and $Cu_9Fe_9S_{16}$ as two metal-rich copper-iron sulfides. *See Id.* In Exhibit B, a 1994 article, the authors generally refer to ZrNbP and $Hf_{1+x}Mo_{1-x}P$ as "metal-rich phosphides" without specifying which of the two metals in the compounds is rich. *See* Exhibit B, page 2962. The abstract of a 1997 article, which is attached as Exhibit C, shows that the authors refer to $Hf_5Nb_5Ni_3P_5$ as a quaternary metal-rich phosphide without identifying which of the three metals is rich. Exhibit C. In Exhibit D, a 1998 article, the authors generally refer to high form pentalandite such as $Fe_{4.5}Ni_{4.5}S_{7.4}$ as metal-rich compositions without identifying which of the two metals is rich. *See* Exhibit D, page 133. For another example, in the 1998 article attached to this paper as Exhibit E, metal-rich polyantimonides $Zr_{7.5}V_{5.5}Sb_{10}$ and $Zr_{6.5}V_{6.5}Sb_{10}$ are described and studied. The term "metal-rich" is used to describe the polyantimonides without referring to any particular metal in the compounds. *See* Exhibit E, page 2219.

Based on the above evidence, it is clear that those skilled in the art would understand what is claimed by each of claims 6-8 and 14 with the term "metal-rich zirconium-aluminium oxycarbonitride," which refers to an oxycarbonitride containing zirconium and aluminium in a total amount more than the total amount of zirconium and aluminium in a corresponding normal stoichiometric oxycarbonitride. It is therefore respectfully submitted that claims 6-8, 14, and 63-71 are all definite under 35 U.S.C. § 112, second paragraph, and are allowable.

35 U.S.C. § 102(b) (Novelty)

Claims 6, 7 and 14 are rejected under 35 U.S.C. 102(b) as being anticipated by Van Hartmetallw Immelbor (DD 288631) or Ver Edelstahlwerke AG (EP 302984 or EP 149449). The Office action rejects these claims by simply stating: "The above references disclose the claimed zirconium-aluminium oxycarbonitride having the claimed amount of aluminium." The rejections are respectfully traversed.

Claim 6 defines a decorative hard coating composition comprising a metal-rich zirconium-aluminium oxycarbonitride and requires that the metal-rich zirconium-aluminium oxycarbonitride has a lower atomic concentration of aluminium than of zirconium. Claim 7 further requires that the atomic concentration of aluminium is less than about one fifth that of zirconium. Claim 14 depends from claim 6. None of DD 288631, EO 302984, and EP 149449 teaches such hard coating compositions.

DD 288631 teaches a coating composition for machine tools consisting of a mixed phase of Al oxycarbides, or oxycarbonitrides of Ti and/or Zr or Hf or a phase mixture of these mixed phases with Al_2O_3 with an Al content of 5-50 wt%. DD 288631 teaches oxycarbonitrides of Ti and/or Zr or Hf, and also teaches that these oxycarbonitrides may be used in combination with Al_2O_3. However, DD 288631 does not teach an oxycarbonitride of zirconium and aluminium,

much less a zirconium-aluminium oxycarbonitride having a lower atomic concentration of aluminium than of zirconium, much less a metal-rich zirconium-aluminium oxycarbonitride. Therefore, DD 288631 cannot anticipate the hard coating composition of claims 6, 7, and 14 of the present application.

EP 302984 or EP 149449 generally teaches a coating composition for hard metal body, especially a cutting tool, that contains an oxycarbonitride of one or more of Ti, Zr, Hf, V, NB, Ta and Cr (preferably Ti or Zr) containing 0.1-2.5 atomic % of aluminum. However, neither EP 302984 nor EP 149449 provides any specific teaching of an Al-Zr oxycarbonitride, and none of the many examples in EP 302984 and EP 149449 actually uses an Al-Zr oxycarbonitride. Even assuming, arguendo, EP 302984 and EP 149449 teaches a coating composition comprising an Al-Zr oxycarbonitride having a lower atomic concentration of aluminium than of zirconium, neither EP 302984 nor EP 149449 discloses, teaches, or suggests a metal-rich oxycarbonitride of any kind. As described in the specification and known to those skilled in the art, metal-rich compounds are completely different from their corresponding normal stoichiometric compounds. The metal-rich zirconium-aluminium oxycarbonitrides of the present application represent a new class of oxycarbonitride materials. Therefore, the hard coating compositions of claims 6, 7, and 14 of the present application are novel and cannot be anticipated by either EP 302984 or EP 149449.

35 U.S.C. §103(a) (Obviousness)

Claims 6-8, 14, and 53 are rejected under 35 U.S.C. 103(a) as being unpatentable over Derflinger et al. (6,827,976) or Gates, Jr. (4,714,660) or Schintlmeister et al. (4,599,281) or Oriental Eng KK (JP 63-060282) for obviousness. Claim 53 has been cancelled, and new claims 63-71 have been added. For reasons detailed blow, Applicants respectfully traverse these rejections.

In order for a 35 U.S.C. §103 rejection to be proper, a *prima facie* case of obviousness must be established. The *MPEP* states:

> To establish a *prima facie* case of obviousness, three basic criteria must be met. First, there must be some suggestion or motivation, either in the references themselves or in the knowledge generally available to one of ordinary skill in the art, to modify the reference or to combine reference teachings. Second, there must be a reasonable expectation of success. Finally, the prior art reference (or references when combined) must teach or suggest all the claim limitations. The teaching or suggestion to make the claimed combination and the reasonable expectation of success must both be found in the prior art, and not based on applicant's disclosure.

MPEP, § 2142 (emphases added). If any of the three criteria is not met, a *prima facie* case has not been established and the 35 U.S.C. §103 rejection must be withdrawn.

The Office action admits that the cited references do not disclose the proportion of the elements in the claimed zirconium aluminum oxycarbonitride, but finds that "Derflinger et al. or Gates, Jr. or Schintlmeister et al. or Oriental Eng KK disclose the claimed zirconium aluminum oxycarbonitride." This finding is not supported by the cited references, however.

The Derflinger reference relates to a method to increase wear resistance of a tool or other machine component. It generally discloses a coating material "selected from the group consisting of nitrides, carbides, oxides, carbonitrides, oxynitrides, and oxycarbonitrides of at least one metal." *See* Abstract. The Derflinger reference also discloses that the at least one metal is "preferably Titanium, Chrominum, Hafniu, Zirconium or Aluminum, preferably two of these metals, particularly preferred Ti and Al and/or Cr and Al." Although the Derflinger reference lists oxycarbonitrides as one of the six kinds of compounds that can be used for the coating materials, no further teaching of oxycarbonitrides is provided. The preferred compounds are TiAlN, CrAlN, and CrN. There is no example of any oxycarbonitride or example of any Zr-Al compound of any kind is provided. According to the case law of the Court of Appeals for the Federal Circuit, the Derflinger

reference actually teaches away from a coating composition comprising a Zr-Al oxycarbonitride. *See In re Baird*, 16 F.3d 380, 382 (Fed. Cir. 1994) (explaining that a prior art reference, which included a broad generic formula that encompassed the claimed composition, "appears to teach away from the selection of [the claimed composition] by focusing on [15] more complex [examples]").

Further, the Derflinger reference does not teach or suggest a metal-rich compound, much less a metal-rich oxycarbonitride. Moreover, the Derflinger reference does not teach or suggest a Zr-Al compound of any kind that contains a lower atomic concentration of Al than of Zr, much less a Zr-Al oxycarbonitride having a lower atomic concentration of Al than of Zr.

Therefore, the Derflinger reference has not only failed to provide all the claim limitations required by claims 6-8 and 14, but also failed to provide any motivation or suggestion to modify the teaching of the Derflinger reference to reach a coating composition comprising a metal-rich Zr-Al oxycarbonitride having a lower atomic concentration of Al than of Zr. And therefore, no prima facie case of obviousness can be established for claims 6-8 and 14 of the present application over the Derflinger reference.

Other references cited by the Office action do not help the deficiencies existing in the teaching of the Derflinger reference, and cannot render claims 6-8 and 14 of the present application obvious either.

For example, none of the Gates reference, the Schintlmeister reference and the Oriental Eng KK reference provides any specific teaching of or an example of Zr-Al oxycarbonitrides. For another example, the Gates reference does not disclose or suggest a metal-rich oxycarbonitride of any kind, much less a metal-rich Zr-Al oxycarbonitride. To the contrary, the Gates reference actually teaches a nitrogen-rich TiAlOCN, which is teaching away from a metal-rich

oxycarbonitride. Similarly, although the Schintlmeister reference generally discloses oxycarbon nitrides of the elements Ti, Zr, Hf, B, Si, Al, it does no teach or suggest a metal-rich compound of any kind. The Oriental Eng KK reference also generally teaches a coating composition containing oxycarbonitrides of one of Si, B, Al, Gp, 4a, 5a, and 6a metals, but it does not teach an oxycarbonitride of both Al and Zr. Neither does the Oriental Eng KK reference teach a metal-rich oxycarbonitride of any kind.

The Office action admits that none of the four cited references teaches a Zr-Al oxycarbonitride having a lower atomic concentration of Al than of Zr, much less a more specific proportion as that claimed in claim 7 or 8. However, the Office action states that it would be obvious to vary the components of the zirconium aluminium oxycarbonitride coating as claimed, "as one would know that varying these components would result in varying properties." This statement has not shown the "suggestion or motivation" as required by the law and MPEP for obviousness rejection. If the reason stated by the Examiner is enough to support an obviousness rejection, there will be no more patentable invention of new materials because all elements on the Periodic Table are known, which are basic components for all materials, and "one would know that varying these components would result in varying properties."

The law is clear that the Examiner could only establish a motivation or suggestion to combine or modify the cited references "by showing some objective teaching in the prior art or that knowledge generally available to one of ordinary skill in the art would lead that individual to combine [or modify] the relevant teachings of the references." *In re Fritch*, 972 F.2d 1260, 1265, 23 USPQ2d 1780, 1783 (Fed. Cir. 1992) (emphasis added); *see also In re Rouffet*, 149 F.3d 1350, 1359, 47 USPQ2d 1453, 1459 (Fed. Cir. 1998) ("The Board must identify specifically ... the reasons one of ordinary skill in the art would have been motivated to select the references

and to combine them to render the claimed invention obvious." (emphasis added)). In the present application, the Examiner has failed to provide any specific reason why a person skilled in the art would have modified the cited references to (1) choose zirconium-aluminium oxycarbonitrides, (2) choose a zirconium-aluminium oxycarbonitride having lower atomic concentration of Al than of Zr, and (3) modify it to be a metal-rich zirconium-aluminium oxycarbonitride. *See In re Lee*, 277 F.3d 1338, 1343-44, 61 USPQ2d 1430 (Fed. Cir. 2002).[2]

Therefore, no prima facie case of obviousness of claims 6-8 and 14 can be established over the cited references, used either separately or in combination.

Thus, for reasons stated above, claims 6-8 and 14 all define patentable subject matter, and should be allowed. Each of the new claims (63-71) depend from claim 6, 7, or 8, and therefore, they are allowable at least for the same reasons as to claims 6-8.

---

[2] What the Examiner suggested is at most that it is "obvious to try" to make a coating composition of the present application, although there was even no "obvious to try" in the cited references. "'Obvious to try' has long been held not to constitute obviousness," and the law has repeatedly rejected that approach. *In re Deuel*, 51 F.3d 1552, 1559, 34 USPQ2d 1210, 1216 (Fed. Cir. 1995).

Conclusion

In view of the above remarks, Applicants respectfully request reconsideration of the present application, and allowance of pending claims (6-8, 14 and 63-71).

The Commissioner is hereby authorized to charge any additional fees or credit any overpayment, to Deposit Account No. 13-0017.

Respectfully submitted,

DATE: September 26, 2006

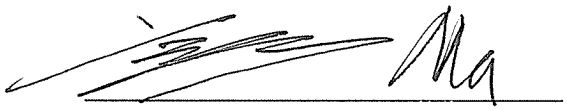

Yufeng Ma
Reg. No. 56,975
Attorney for Applicants

McAndrews, Held & Malloy, Ltd.
500 W. Madison, 34th Floor
Chicago, IL 60661
Telephone: (312) 775-8000
Facsimile: (312) 775-8100

Exhibit A

Canadian Mineralogist
Vol. 14, pp. 529-535 (1976)

THE CRYSTAL STRUCTURE OF MAWSONITE, $Cu_6Fe_2SnS_8$

J. T. SZYMAŃSKI

Mineral Sciences Laboratory, CANMET, Department of Energy, Mines and Resources
555 Booth Street, Ottawa, Canada

ABSTRACT

The crystal structure of mawsonite, $Cu_6Fe_2SnS_8$, has been determined and refined to an *R*-value of 0.049 (all 1426 data) and 0.037 (1004 "observed" data only) from multiple sets of four-circle diffractometer X-ray intensity data. Microprobe analysis indicates that the formula is stoichiometric in terms of the metals, but with 1.5% of the sulfur replaced by selenium in the specimen examined. The structure is tetragonal, *a* 7.603(2), *c* 5.358(1)Å, space group $P\bar{4}m2$, and is based on a nearly *ccp* sulfur matrix with metals filling half of the tetrahedral interstices and an extra interstitial Fe atom at the (½,½,½) position. The latter gives rise to close Fe . . . Fe . . . Fe contacts (2.679(1)Å) in the *z* direction, but no close Fe . . . Fe contacts normal to this. The deviations from an ideal *ccp* structure are due to the large Sn atom at the origin, and the extra Fe atom at ½,½,½. The bond lengths, angles and thermal parameters are in close agreement with those found in stannite, $Cu_2(Fe,Zn)SnS_4$, and kesterite, $Cu_2(Zn,Fe)SnS_4$.

SOMMAIRE

La structure cristalline de la mawsonite, $Cu_6Fe_2SnS_8$, a été déterminée et affinée jusqu'à un indice *R* de 0.049 (pour toutes les 1426 données) et de 0.037 (pour les 1004 données "observées", seulement) au moyen de plusieurs séries de données d'intensité recueillies sur diffractomètre aux rayons X à quatre cercles. L'analyse à la microsonde indique que la formule est stoechiométrique en ce qui concerne les métaux, mais que 1.5% du soufre contenu dans l'échantillon étudié est remplacé par du sélénium. La structure est tétragonale, *a* 7.603(8), *c* 5.358(1)Å, dans le groupe spatial $P\bar{4}m2$; elle consiste en un assemblage quasi-cubique compact d'atomes de soufre, dont les interstices tétraédriques sont remplis pour moitié par les métaux tandis qu'un atome de fer supplémentaire est interstitiel en position (½,½,½). Celui-ci donne lieu à de courtes distances Fe . . . Fe . . . Fe (2.679(1)Å) dans la direction *z*, mais non perpendiculairement à cette direction. La structure s'écarte de la structure idéale à empilement cubique compact; deux atomes en sont la cause: le gros atome Sn à l'origine et l'atome Fe en ½,½,½. Les valeurs des longueurs de liaison, des angles et des paramètres thermiques concordent avec celles que l'on observe dans la stannite $Cu_2(Fe,Zn)SnS_4$ et la kestérite $Cu_2(Zn,Fe)SnS_4$.

INTRODUCTION

Mawsonite, $Cu_6Fe_2SnS_8$, was first described by Markham & Lawrence (1965), and identified by them as being present in the material described as "orange bornite" by Murdock (1916). The chemical composition has been variously reported as $Cu_7Fe_2SnS_{10}$ (Markham & Lawrence 1965), $Cu_{5.91}Fe_{1.89}Sn_{0.98}S_{8.20}$ (Lévy 1967), $Cu_6Fe_2SnS_8$ (Springer 1968), and $Cu_{2.86}FeSn_{0.55}S_{4.06}$ (Kachalovskaya *et al.* 1973). The more recent analyses of Petruk (1973) and of Yamanaka & Kato (1976) are in agreement with the present analyses and with the present structural determination.

Mawsonite powder patterns generally have been indexed on a pseudo-cubic cell, *a* 10.74± .01Å, but because of its anisotropic optical properties, mawsonite cannot be truly cubic (Markham & Lawrence 1965). Recently, Yamanaka & Kato (1976) have indexed the mawsonite pattern using a tetragonal cell, *a* 10.745, *c* 10.711Å.

Structural examination of mawsonite was undertaken in our laboratory, to provide accurate information on a metal-rich copper-iron-tin sulfide mineral, for comparison with the related non metal-rich minerals, stannite and kesterite (Hall *et al.* 1975), in the same way that the chalcopyrite series of minerals was investigated (Hall 1975). In the latter series, two metal-rich copper-iron sulfides, haycockite, $Cu_4Fe_5S_8$, and mooihoekite, $Cu_9Fe_9S_{16}$, were both believed to have iron atoms filling additional tetrahedral interstices, though it was difficult to prove this unequivocally. It was hoped that the present investigation would indicate more clearly the preference of iron over copper to occupy additional interstitial sites.

EXPERIMENTAL

Three single-crystal fragments of mawsonite were successively examined by microprobe analysis and crystal structure determination. The first two fragments proved to be too small for an accurate parameter refinement, though the structure was solved using these data. The results of the third crystal structure determination,

TABLE 1. MICROPROBE ANALYSES FOR MAWSONITE

Element	Specimen 1		Specimen 2		Specimen 3	
	Wt.%	Formula	Wt.%	Formula	Wt.%	Formula
Cu	43.2	5.89	42.8	5.89	44.0	6.02
Sn	13.8	1.01	13.8	1.01	13.7	1.01
Fe	13.1	2.02	13.0	2.03	12.9	2.02
S	29.8	8.07	29.2	7.95	28.8	7.83
Se	-	-	1.0	0.11	1.1	0.12
Total	99.9		99.8		100.5	

Specimen 1. Hotuko vein, Kanagase 1 Kuno mine, Hyogo Prefecture, Japan (Smithsonian Institute, Specimen #122102).
Specimens 2, 3: Kidd Creek mine, Timmins, Ontario.

on a mawsonite specimen from the Kidd Creek mine, Timmins, Ontario, are reported here.

The microprobe analyses for the three mawsonite specimens examined are listed in Table 1. The second and third were found to have a small but significant quantity of selenium replacing sulfur. This appears to be the first established occurrence of selenium in mawsonite.

The third specimen of mawsonite, after extraction from a polished section, was cut with a knife, to provide more regular "faces" so as to facilitate subsequent absorption corrections. The resultant fragment was an irregular hexagonal tablet $0.3\times0.2\times0.005$ mm. Gandolfi powder photographs of the single crystal were the same as those previously published for mawsonite (Markham & Lawrence 1965), and contained no additional lines that could be attributed to impurities.

The crystal was mounted on a four-circle automatic diffractometer in a general orientation. The cell dimensions were determined from a least-squares refinement of the 2θ, χ and ω angles (Busing 1970) for 90 reflections in the range $55°<2\theta<93°$. The parameters were refined on a triclinic cell. The difference between the a and b cell edges was less than 0.2σ, and the maximum deviation from orthogonality was less than 1′ of arc. The errors quoted in the Table 2 represent 3σ as derived from the least-squares matrix. Long-exposure precession photographs, and diffractometer traces of weak axial reflections showed that there were no systematic absences. Comparison of absorption-corrected intensities of symmetry-related reflections showed that the Laue symmetry of the lattice was $4/mmm$ and not $4/m$.

Five Friedel-equivalent segments of data, each 1/16 of the Ewald sphere, were collected using monochromatized Mo$K\alpha$ radiation to a limit of $2\theta=120°$. The scan range was 1.9° plus the α_1–α_2 dispersion, and the background counts were measured on either side of the peak for a total time approximately equal to the average

TABLE 2. CRYSTAL DATA FOR MAWSONITE, $Cu_6Fe_2SnS_8$

Composition: (microprobe analysis given in Table 1)

Source: Kidd Creek mine, Timmins, Ontario

Formula weight: 868.1

Crystal system: tetragonal

Systematic absences: none

Space group: (possibly) $P422$(#89), $P4mm$(#99), $P\bar{4}2m$(#111), $P\bar{4}m2$(#115), $P4/mmm$(#123)
$P\bar{4}m2$(#115) confirmed by structure analysis.

Cell dimensions: $a = 7.603(2)$, $c = 5.358(1)$Å at 20°C using $\lambda(MoK\alpha_1) = 0.70926$Å

Linear absorption coefficient: $\mu(MoK\alpha) = 160.3$ cm^{-1}

Density: $D_{calc} = 4.65$g/cm^{-3}; $Z = 1$
(Density not measured)

scan time. Three standards were measured after every 50 reflections to maintain a check on crystal alignment and instrument stability. A uniform systematic decrease of about 4% of the intensity of the standards was noted over the period of data collection, and as the crystal alignment was found to be unchanged at the end, a linear scaling procedure was applied to the data to account for this decrease.

Absorption corrections were applied to the intensity data using a Gaussian integration procedure, and the five equivalent segments were averaged and reduced to a single data set which contained 1426 independent intensities, of which 1004 can be considered as observed at the 10% significance level, i.e. $I(\text{net})\geqq1.65\sigma(I)$. The discrepancy factor ($\Sigma\Delta I/\Sigma I$) among the five data sets was 0.031.

Structure Solution and Refinement

Examination of the cell dimensions suggested that the structure was based on two sphalerite-type 5.3Å "cubes", with the tetragonal cell dimension a, representing the face diagonal of the "cube". This reasoning imposed the condition that the nearly *ccp* sulfur lattice would be approximately *c*-centred and would have $\bar{4}$ symmetry about the *c*-axis (and hence about a line through the mid-point of the *c*-face). An added condition for limiting the choice of space group was that, based upon the probable value of $Z=1$ (i.e. one formula unit per unit cell to account for a reasonable value of D_{calc}), the space group chosen would have to have a site with an equivalent-position multiplicity of 1, where tin could be assigned. Examination of the seven possible space groups for equivalent position sites that would yield an approximately *ccp* sulfur lattice with normal S . . . S distances of about 3.8Å, eliminated all except $P\bar{4}m2$, and this

choice led to a successful solution of the structure.

The sulfur atoms were assigned to sites 4*j* (~¼,0,~¼) and 4*k* (~¼,½,~¼) and various combinations were tried in assigning the metals to the tetrahedral interstices of the sulfur matrix. The tin atom was arbitrarily assigned to the origin, and an "average" metal (¾Cu+¼Fe) was assigned to fill the tetrahedral vacancies at sites 4*i* (~¼,~¼,½), 2*g* (0,½,~0) and 1*b* (½,½,0). This model refined successfully, but the difference synthesis indicated that an extra interstitial atom was required at site 1*c* (½,½,½). Bearing in mind the multiplicities of these sites and the stoichiometry of the formula (6Cu+2Fe), site 4*i* was assigned as copper. This left two copper and two iron atoms to be assigned to the four sites 2*g*, 1*b* and 1*c*. Better agreement was observed when copper was placed at site 2*g* and two iron atoms at sites 1*b* and 1*c*, than when the metal types were reversed.

The final correct model refined anisotropically to $R=0.037$ for the 1004 observed reflections (see above) and to $R=0.049$ when all 1426 were treated as observed. There was no significant difference in the final parameters between these two refinements, and the parameters quoted in Table 3 are those for the latter case. An isotropic extinction parameter (Larsen 1970) was included in the refinement. The scattering curves used were those for the neutral atomic species Cu,Fe,Sn,Se and S, taken from Cromer & Mann (1968) and the anomalous dispersion corrections were those of Cromer & Libermann (1970). Better agreement was obtained using the curves for the neutral atomic species than for the ionized species. This is opposite to what was found in the refinement of chalcopyrite (Hall & Stewart 1973), but the same as that found in the refinements of stannite and kesterite (Hall & Stewart 1975). In the final stages of refinement, a composite curve ($0.985f_S$ $0.015f_{Se}$) was used to account for the 1.5% selenium replacement of sulfur in the sample. The anomalous scattering was also modified to take this into account. The resultant improvement in the agreement factor was 0.001, but it appears to be significant. In the least-squares procedure, refinement using unit weights and calculated weights was tried, (calculated weight $= 1/\sigma^2(F)$, where $\sigma(F)$ is based on the relative agreement of the five observations of the intensity and on counting statistics. No significant difference was observed between these refinements, and the results quoted are based on the unit-weight refinement.

The calculations were carried out using the X-ray system of programs (Stewart *et al.* 1972). The bond lengths and angles are given in Table 4. The observed ($10\times F_o$) and calculated ($10\times F_c$) structure factors are given in Table 5*, for the refinement treating all data as "observed", though reflections which can be considered "unobserved" (see above) are marked with an asterisk.

Description of the Structure and Discussion

The structure of mawsonite is based upon the compounding of two sphalerite-like cubes (Fig. 1). Kesterite and stannite (Hall & Stewart 1975) also have "two cube" structures, but in these the doubling of the cell occurs along the *z*-direction. In mawsonite, the expansion is accomplished by considering the face diagonals of two adjacent sphalerite-like cubes as the a_1, a_2 directions of the tetragonal cell. The sulfur matrix is approximately cubic close-packed, with metal atoms occupying half of the available tetrahedral interstices, and an additional metal atom (Fe2) occupying the interstice at the (½,½,½) position of the cell. This results in a coordination scheme in which each metal is in contact with four sulfur atoms (Fig. 2, a-e),

*Table 5 is available, at a nominal charge, from the Depository of Unpublished Data, CISTI, National Research Council of Canada, Ottawa, Canada, K1A 0S2.

TABLE 3. ATOMIC POSITIONAL AND THERMAL PARAMETERS.

The anisotropic temperature factors are expressed in the form $T = \exp[-2\pi^2(U_{11}a^{*2}h^2 + 2U_{12}a^*b^*hk + \ldots]$, and the values quoted are x 10^4.

Atom	Site	x	y	z	U_{11}	U_{22}	U_{33}	U_{12}	U_{13}	U_{23}	B(equiv.)
Sn	1*a*	0	0	0	84(1)	84(1)	91(1)	0	0	0	0.68
Cu1	2*g*	½	0	0.0002(6)	165(3)	247(4)	186(3)	0	0	0	1.57
Cu2	4*i*	0.2463(1)	0.2463(1)	½	165(1)	165(1)	182(2)	-27(2)	12(4)	-12(4)	1.35
Fe1	1*b*	½	½	0	114(2)	114(2)	51(2)	0	0	0	0.73
Fe2	1*c*	½	½	½	83(2)	83(2)	54(2)	0	0	0	0.58
S1	4*j*	0.2615(2)	0	0.2538(3)	95(3)	106(3)	115(4)	0	-26(3)	0	0.83
S2	4*k*	0.2597(2)	½	0.2490(2)	92(3)	132(4)	84(3)	0	-18(3)	0	0.81

TABLE 4. BOND DISTANCES AND ANGLES WITH STANDARD DEVIATIONS

(a) Bond distances (Å)

Sn	- S1	2.409(1)
Cu1	- S1	2.266(2)
Cu1	- S2	2.384(2)
Cu2	- S1	2.293(1)
Cu2	- S2	2.354(1)
Fe1	- S2	2.262(1)
Fe2	- S2	2.269(1)

(b) Non-bonded short metal-metal distances (Å)

Cu2...Fe2		2.728(1)
Fe1...Fe2		2.679(1)

(c) Sulfur tetrahedra (Å)

1. Around Sn

S1	... $S1^{9}$	3.977(2)
S1	... $S1^{23}$	3.912(2)

2. Around Cu1

S1	... $S1^{7}$	3.626(2)
$S2^{23}$	... $S2^{28}$	3.949(2)
S1	... $S2^{23}$	3.801(2)

3. Around Cu2

S1	... S2	3.802(1)
S1	... $S2^{22}$	3.779(2)
S1	... $S1^{22}$	3.856(2)
S2	... $S2^{22}$	3.730(2)

4. Around Fe1, Fe2

S2	... $S2^{7}$	3.654(2)
S2	... $S2^{23}$	3.714(2)

(d) Bond Angles (°)

S1	- Sn -	$S1^{9}$	111.26(5)
S1	- Sn -	$S1^{23}$	108.59(3)
S1	- Cu1 -	$S1^{7}$	106.30(13)
S1	- Cu1 -	$S2^{23}$	109.63(3)
$S2^{23}$	- Cu1 -	$S2^{28}$	111.86(13)
S1	- Cu2 -	S2	109.78(5)
S1	- Cu2 -	$S1^{22}$	114.41(5)
S1	- Cu2 -	$S2^{22}$	108.82(5)
S2	- Cu2 -	$S2^{22}$	104.81(4)
S2	- Fe1 -	$S2^{7}$	107.73(5)
S2	- Fe1 -	$S2^{26}$	110.35(3)
S2	- Fe2 -	$S2^{7}$	107.28(5)
S2	- Fe2 -	$S2^{25}$	110.58(3)
Sn	- S1 -	Cu1	108.78(9)
Sn	- S1 -	Cu2	106.44(4)
Cu1	- S1 -	Cu2	112.67(5)
Cu2	- S1 -	$Cu2^{23}$	109.48(6)
Fe1	- S2 -	$Cu1^{23}$	109.80(8)
Fe1	- S2 -	Cu2	111.84(4)
Fe1	- S2 -	Fe2	72.50(4)
Fe2	- S2 -	Cu2	72.31(3)
Fe2	- S2 -	$Cu1^{23}$	177.71(8)
Cu2	- S2 -	$Cu2^{11}$	110.07(6)
Cu2	- S2 -	$Cu1^{23}$	106.51(5)

List of superscripts, indicating symmetry operations, used in text, Table, and Fig. 2.

7.	1-x, y, z	23.	y, x, -z
9.	-x, y, z	25.	y, 1-x, 1-z
11.	x, 1-y, z	26.	y, 1-x, -z
13.	x, -y, z	28.	y, -x, -z
22.	y, x, 1-z		

one of the sulfur atoms (S1) is coordinated to four metals (Fig. 2f), and the other sulfur atom (S2), is coordinated to five metals, due to the presence of the extra metal (Fe2), (Fig. 2g).

The additional iron atom (Fe2) has four coordinating sulfur atoms (S2) in a distorted tetrahedron at a distance of 2.269Å (Fig. 2e), and has six metal atoms at close distances. The Fe1 atom is directly above and below it at 2.679Å, and four Cu2 atoms at 2.728Å complete the flattened octahedron of metal nearest-neighbors. Such an environment is common in the "stuffed derivatives" (structures with extra interstitial metals) in the chalcopyrite series (Hall 1975). The structure of mooihoekite (Hall & Rowland 1973) is very similar to that of mawsonite. Like mawsonite, mooihoekite ($Cu_9Fe_9S_{16}$) has a metal/sulfur ratio of 9/8, but because the cell is approximately twice that of mawsonite, it contains two extra atoms. Both of these extra metal sites are filled by iron atoms, but these sites are not equivalent. In one case they give rise to infinite chains in the *z*-direction of Fe . . . Fe . . . Fe . . . atoms 2.69Å apart, and in the second case the chains are . . Cu . . . Fe . . . Cu . . . Fe . . ., also 2.69Å apart. In mawsonite, the single extra iron atom gives rise to infinite chains . . Fe1 . . . Fe2 . . . Fe1 . . . Fe2 . . . 2.68Å apart.

Mawsonite was originally reported as being "magnetic", (Markham & Lawrence), and the largest crystal specimen used here was tested with iron wire, and a strong bar magnet. The crystal was unaffected by the iron wire, but was attracted weakly by the magnet. The iron atoms in the structure are close enough for magnetic

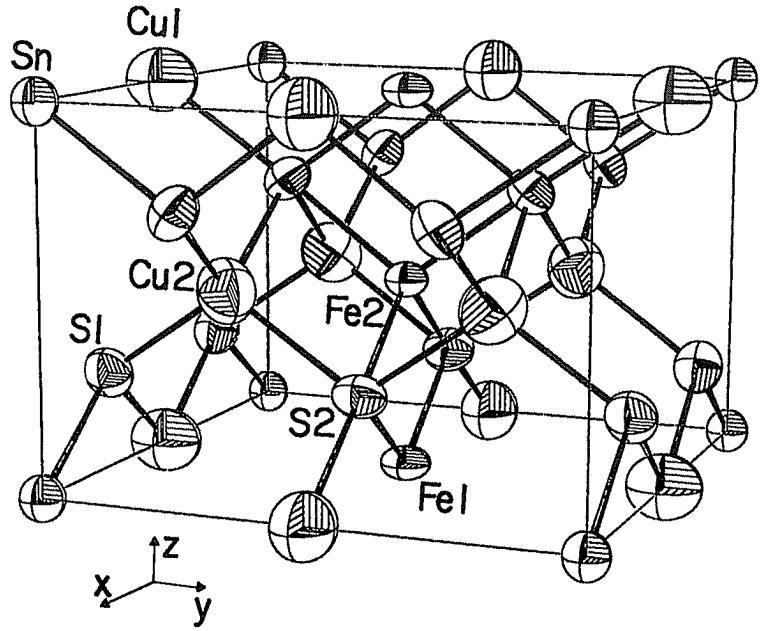

FIG. 1. The unit cell of mawsonite. Thermal ellipsoids are drawn to include 99% probability.

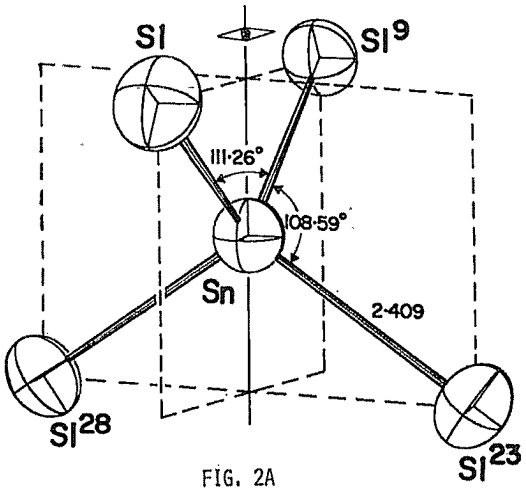

FIG. 2A

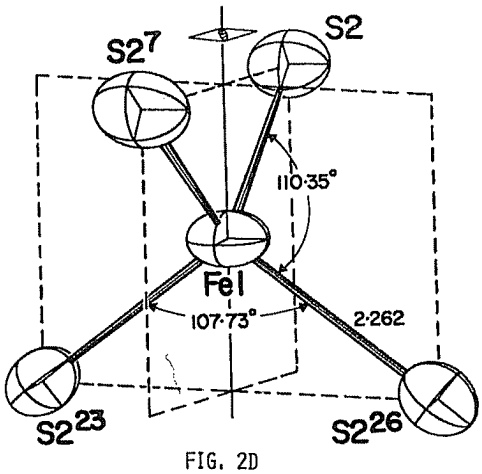

FIG. 2D

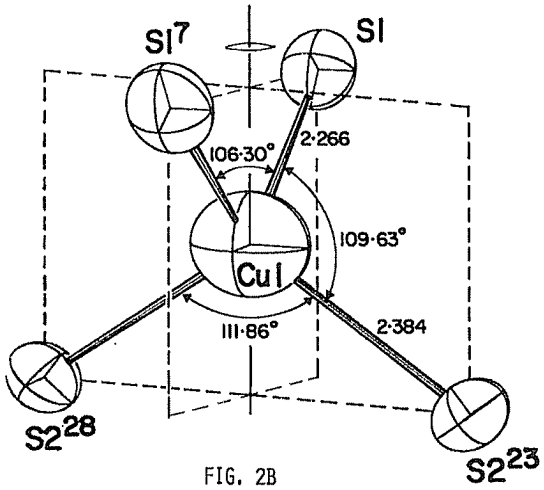

FIG. 2B

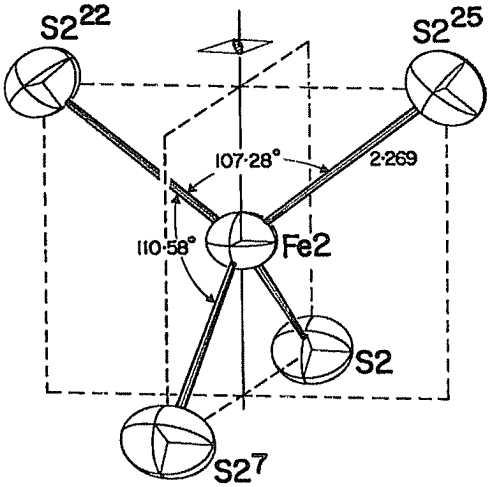

FIG. 2E

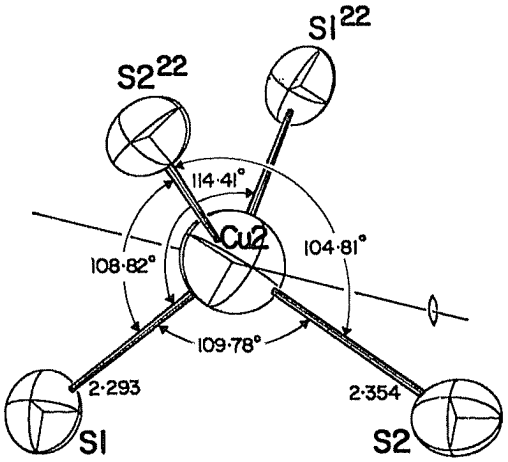

FIG. 2C

FIG. 2. Metal-sulfur coordination tetrahedra: (A) around Sn; (B) around Cul; (C) around Cu2; (D) around Fel; (E) around Fe2; (on page opposite): sulfur-metal coordination polyhedra; (F) around Sl; (G) around S2.

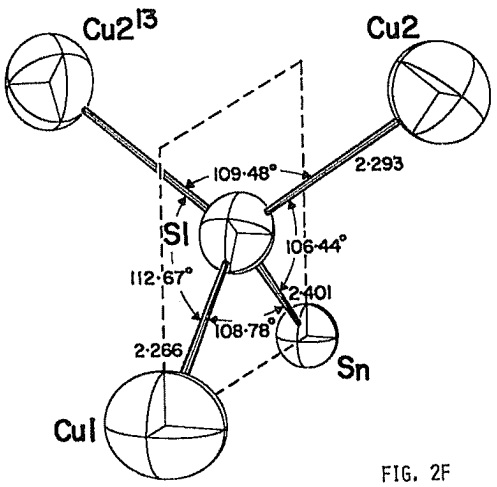

FIG. 2F

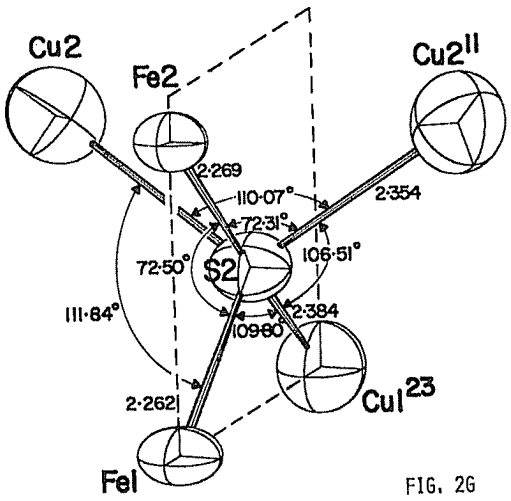

FIG. 2G

interaction in the *z*-direction to occur, probably via the nearest sulfur atoms (S2). However, such a -Fe-S-Fe-S- interaction can only be one-dimensional in the case of mawsonite as the distance between the iron "chains" is too large (7.603Å). Similar one-dimensional systems are known, e.g., $CsCoCl_3 \cdot 2H_2O$ and $RbFeSl_3$; the latter has inter- and intra-chain distances very close to those found in mawsonite, and both $CsCoCl_3 \cdot 2H_2O$ and $RbFeCl_3$ have very low Néel temperatures.

The deviations of the coordination tetrahedra from ideal geometry can be accounted for in terms of two factors: (1) the additional iron metal at the (½,½,½) position results in some degree of "crowding" around the five-coordinate S2 atom, with consequent distortions of all angles involving S2; (2) the larger tin atom at the origin gives rise to a displacement of the coordinating sulfurs away from this position. The Sn-S bond length (2.409Å) is very close to those found in stannite (2.411Å) and kesterite (2.408Å) (Hall *et al.* 1975) and is much larger than any of the other metal-sulfur distances in the structure. The sulfur atoms are moved away from tin much more in the *x*-*y* plane than in the *z*-direction, and this results in a "flattened" tetrahedron, with the S1-S1-S1[9] angle opened up to 111.26°, and the S1-Sn-S1[23] angle compressed to 108.59° from the ideal value of 109.47°.

The thermal parameters for all the atoms are in close agreement with those found in stannite and kesterite, and follow the general pattern observed in the chalcopyrite series [$\overline{B}$(Cu)>$\overline{B}$(Fe)], except that the magnitudes of $\overline{B}$(Fe) observed here are less than in the chalcopyrite series. This is probably due to the "crowding" occurring around the centre of the mawsonite cell. This factor also explains why $\overline{B}$(Fe2) and $\overline{B}$(Cu2) are less than $\overline{B}$(Fel) and $\overline{B}$(Cul) respectively.

The cell parameters obtained in this work [*a* 7.603(2), *c* 5.358(1)Å] are slightly, but not significantly larger than the reduced cell of Yamanaka & Kato (1976); *a* 7.598(1), *c* 5.355 (3)Å. It is probable that the selenium replacement of some sulfur in the present mawsonite specimen results in the fractionally larger cell parameters.

Powder Diffraction Pattern

Long-exposure Gandolfi single-crystal powder photographs were obtained for the crystal used in the structure determination. After the structure was solved and refined, the computer program POWGEN (Hall & Szymański 1975) was run. This program calculates the X-ray powder pattern using either the observed or the calculated single-crystal intensities, for either a specific wavelength or combination of wavelengths. The Gandolfi pattern was compared to the calculated pattern, and excellent agreement was found.

However, serious discrepancies were observed between these two patterns and the recently published mawsonite powder pattern of Yamanaka & Kato (1976). Their lines observed at d=7.60 (hkl=100), 2.461(102) and 1.319(104) have such weak calculated and observed single-crystal intensities that they should not have been observable. Their line at d=1.302(512) is too strong to be due to mawsonite alone, and also, their line at d=3.388, which was not observed on the Gandolfi films, cannot be indexed using the true mawsonite cell. It seems that despite

their careful purification procedures, their mawsonite specimen may have contained extraneous material.

Table 6 gives the X-ray powder pattern for mawsonite obtained from the single-crystal observed intensities.

TABLE 6. X-RAY POWDER PATTERN OF MAWSONITE CALCULATED FOR CoKα RADIATION FROM OBSERVED SINGLE-CRYSTAL DIFFRACTOMETER INTENSITIES

d(Å)	I_{calc}	hkl	d(Å)	I_{calc}	hkl
5.37	11	110,001	1.619	43	421,203
4.38	14	101	1.581	2	213
3.800	6	200,111	1.550	6	402
3.100	100	201	1.462	3	431,303
2.871	13	211	1.365	3	521,323
2.683	26	220,002	1.341	13	440,004
2.401	6	310,112	1.303	1	512
2.291	4	301	1.232	20	601,423
2.190	2	202	1.201	9b	620,442,224
1.962	3	321	1.096	34	622,404
1.899	70	400,222	1.033	22	641,603,205
1.790	3	330,312	0.949	25	800,444
1.742	3	411,103			

Acknowledgements

The author is grateful to Mr. D. R. Owens of this Division for the microprobe analyses, to Dr. S. R. Hall, formerly of this Division, for useful comments and discussion and to Dr. R. I. Thorpe of the Geological Survey of Canada for the two mawsonite specimens from the Kidd Creek mine, Timmins, Ontario. The first specimen was by courtesy of Mr. J. S. White Jr., Smithsonian Institution, Washington, D.C. The diagrams were prepared using a modified version of the program ORTEP2 (Johnson 1965).

References

Busing, W. R. (1970): Least-squares refinement of lattice and orientation parameters for use in automatic diffractometry. *In* Crystallographic Computing (F. R. Ahmed, ed.), 319-330. Copenhagen: Munksgaard.

Cromer, D. T. & Mann, J. B. (1968): X-ray scattering factors computed from numerical Hartree-Fock wave functions. *Acta Cryst.* **A24**, 321-324.

——— & Libermann, D. (1970): Relativistic calculation of anomalous scattering factors for X-rays. *J. Chem. Phys.* **53**, 1891-1898.

Hall, S. R. (1975): Crystal structures of the chalcopyrite series. *Can. Mineral.* **13**, 168-172.

——— & Stewart, J. M. (1973): The crystal structure refinement of chalcopyrite, $CuFeS_2$. *Acta Cryst.* **B29**, 579-585.

——— & Rowland, J. F. (1973): The crystal structure of synthetic mooihoekite, $Cu_9Fe_9S_{16}$. *Acta Cryst.* **B29**, 2365-2372.

——— & Szymański, J. T. (1975): Paper F13, Powder pattern generation from single crystal data. Winter Meet. *Amer. Cryst. Assoc.*, Charlottesville, Va.

———, Kissin, S. A. & Stewart, J. M. (1975): Paper 04.1-24, Stannite and kesterite: distinct minerals or components of a solid solution. *Acta Cryst.* **A31**, Part S3, S67.

Johnson, C. K. (1970): ORTEP: A FORTRAN thermal-ellipsoid plot program for crystal structure illustrations. *Rep.* **ORNL-3794, 2nd Revision** ORTEP-II addition 1971, *Oak Ridge Nat. Lab.*, Oak Ridge, Tennessee. The Johnson program has been modified for use in the X-RAY STEWART System by J. F. Guédon, S. Hall, P. Richard and S. Whitlow, 1974.

Kachalovskaya, V. M., Osipov, B. S., Kukoev, V. A., Kozlova, E. V. & Basova, G. V. (1973): Mawsonite and stannoidite from the bornite ores of the Urup deposit. *In* Miner. Paragenezisy Miner. Rud. Mestorozhd (P. M. Tamarinov, ed.). Nauka, Leningrad.

Larson, A. C. (1970): The inclusion of secondary extinction in least-squares refinement of crystal structures. *In* Crystallographic computing (F. R. Ahmed, ed.), 291-294. Copenhagen: Munksgaard.

Lévy, C. C. (1967): Contribution à la minéralogie des sulfures de cuivre du type Cu_3XS_4. *Mén. Bur. Recherches Géol. Minières* **54**, 35-74.

Markham, N. L. & Lawrence, L. J. (1965): Mawsonite, a new copper–iron–tin sulphide from Mt. Lyell, Tasmania and Gingha, New South Wales. *Amer. Mineral.* **50**, 900-908.

Murdoch, J. (1916): *Microscopical Determination of the Opaque Minerals.* McGraw-Hill, New York.

Petruk, W. (1973): Tin sulphides from the deposit of Brunswick Tin Mines Limited. *Can. Mineral.* **12**, 46-54.

Springer G. (1968): Electronprobe analyses of stannite and related tin minerals. *Mineral. Mag.* **36**, 1045-1051.

Stewart, J. M., Kruger, G., Ammon, H., Dickinson, C. H. & Hall, S. R. (1972): The X-ray system of crystallographic programs. *Univ. Maryland Comp. Sci. Tech. Rep.* **TR-192.**

Yamanaka, T. & Kato, A. (1976): Mössbauer effect study of ^{57}Fe and ^{119}Sn in stannite, stannoidite and mawsonite. *Amer. Mineral.* **61**, 260-265.

Manuscript received May 1976, emended June 1976.

Exhibit B

Ternary Metal-Rich Phosphides: Structure, Bonding, and Site Preferences in ZrNbP and $Hf_{1+x}Mo_{1-x}P$

Gordon J. Miller* and Jun Cheng

Department of Chemistry and Ames Laboratory/DOE, Iowa State University, Ames, Iowa 50011

Received November 10, 1994[⊗]

Semiempirical electronic structure calculations are utilized to assess the bonding and metal atom arrangement in the recently discovered ternary phosphide ZrNbP, which adopts the Co_2Si structure type. These same calculations reveal that ZrMoP should form in the Fe_2P structure type due primarily to metal−metal interactions within each system. Related structural alternatives like the Cu_2Sb-type and the Ni_2In-type are also examined for their stability ranges as a function of valence electron concentration (vec). Synthesis and structural characterization of $Hf_{1.06}Mo_{0.94}P$ by single-crystal X-ray diffraction are also reported and confirm the prediction of stability of the Fe_2P structure type for this vec. $Hf_{1.06}Mo_{0.94}P$ crystallizes in the space group $P\bar{6}2m$ (No. 189); $a = 6.8954(4)$ Å; $c = 3.4164(4)$ Å; $Z = 3$; $R = 0.024$; $R_w = 0.027$ ($I \geq 3\sigma(I)$).

The chemistry of transition metal-rich chalcogenides has been receiving increasing attention due to the fascinating structures and metal atom ordering phenomena among mixed-metal sulfides and selenides.[1] Ternary phosphides also comprise an important fundamental class of refractory compounds, but these generally involve the combination of an early transition metal (Zr, Nb, Mo) with a late transition metal, generally from the 3d series (Fe, Co, Ni).[2] Rarely have mixed early transition metal phosphides been isolated and structurally characterized.

The recent report of the Co_2Si structure type (C37-type from *Strukturbericht*; oP12[3]) for ZrNbP[4] is, perhaps, somewhat surprising, given that metal-rich compounds of this type generally form other, quite complex structure types, e.g., Zr_2P[5] (oC108) and Nb_2P[6] (oP54). These contain some metal atoms in local environments that are similar to a body-centered cubic (bcc) arrangement. Another surprising aspect of ZrNbP is the clear separation of Zr and Nb into different crystallographic sites with no evidence for mixed site occupations nor of any variable compositions, $Zr_{1\pm x}Nb_{1\mp x}P$. This compound differs from the (Ta, Nb) sulfides, in which there is an incomplete segregation of Nb and Ta atoms into inequivalent sites, but is similar to them in that these ternary sulfides occur only for specific Ta:Nb ratios.

In this article, we examine the electronic structure of the Co_2Si structure type using the metals Zr, Nb, and Mo with P in order to assess the electronic influences on metal segregation and minimal homogeneity width. We also address the preference of the Co_2Si structure over related structure types for compounds with valence electron concentrations (vec's) near ZrNbP. These calculations led to an investigation of more electron rich systems and the discovery of the Fe_2P-type structure in the (Hf,Mo)P system. The syntheses of these compounds and the single-crystal structural determination of $Hf_{1.06}Mo_{0.94}P$ will also be presented.

The Co_2Si Structure Type

Much has been written regarding the Co_2Si structure type.[7] Other designations include $PbCl_2$ (C23-type) and SrH_2 (C29-type), but Hyde et al.[7] recently pointed out that there should be no distinction between the C23- and C29-types. Each of these compounds adopts the same space group, *Pnma*, with three atoms in the asymmetric unit occupying 4*c* Wyckoff sites (x_i, $^1/_4$, z_i). However, differences in the ratios of the lattice constants *a*/*b* and *c*/*b* (*b* = shortest lattice parameter) indicate that these different designations are indeed appropriate to describe the flexibility allowed by the orthorhombic symmetry. Hulliger has also demonstrated the relationship between Co_2Si (C37) and Ni_2In ($B8_b$-type).[8]

Jeitschko,[9] Flahaut and Thévet,[10] and Hyde et al.[7] have independently constructed sorting diagrams using various lattice parameter ratios. Their results identify at least two primary regimes, although the "borders" are not well defined. Nevertheless, the Co_2Si (C37) regime corresponds to $1.80 \leq c/b \leq 2.20$ and $1.25 \leq a/b \leq 1.40$ whereas the $PbCl_2$ (C23) regime occurs for $1.60 \leq c/b \leq 2.50$ and $1.50 \leq a/b \leq 1.90$. Clearly, the *a*/*b* ratio is the significant parameter for this segregation. In general, the difference between the $PbCl_2$ and Co_2Si structure types is noted when the coordination numbers of the majority components in binary compounds are examined. In the $PbCl_2$ structure, these coordination numbers are unequivocally 4 (tetrahedral) and 5 (square pyramidal) whereas, in the Co_2Si structure, these values tend to increase by the addition of capping atoms: i.e., the coordination polyhedra resemble trigonal bipyramids and octahedra. In the Ni_2In ($B8_b$) structure, this trend is completed with the coordination numbers 5 (trigonal bipyramidal) and 6

[⊗] Abstract published in *Advance ACS Abstracts*, May 1, 1995.

(1) (a) Harbrecht, B.; Franzen, H. F. *Z. Anorg. Allg. Chem.* **1987**, *551*, 74. (b) Harbrecht, B. *Z. Kristallogr.* **1988**, *182*, 118. (c) Harbrecht, B.; Franzen, H. F. *Z. Kristallogr.* **1989**, *186*, 119. (d) Yao, X.; Franzen, H. F. *J. Less-Common Met.* **1990**, *161*, L37. (e) Yao, X.; Franzen, H. F. *J. Solid State Chem.* **1990**, *86*, 88. (f) Yao, X.; Franzen, H. F. *Z. Anorg. Allg. Chem.* **1991**, *598*, 353. (g) Yao, X.; Franzen, H. F. *J. Am. Chem. Soc.* **1991**, *113*, 1426. (h) Yao, X.; Miller G. J.; Franzen, H. F.; *J. Alloys Comp.* **1992**, *183*, 7.

(2) Villars, P.; Calvert, L. D. *Pearson's Handbook of Crystallographic Data for Intermetallic Phases*; American Society for Metals: Metals Park, OH, 1985; Vol 3.

(3) This notation is called the Pearson symbol: oP12 means orthorhombic crystal class, Primitive unit cell setting, 12 atoms in the unit cell. See: Pearson, W. B. *Crystal Chemistry and Physics of Metals and Alloys*; Wiley: New York, 1972.

(4) Marking, G.; Franzen, H. F. *J. Alloys Comp.* **1994**, *204*, L16.

(5) Ahlzén, P.-J.; Rundqvist, S. *Z. Kristallogr.* **1989**, *189*, 117.

(6) Kuzma, Yu. B.; Orishchin, S. V.; Lomnitskaya, Ya. F., Glov'jak, T. *Dopov. Akad. Nauk Ukr. RSR, Ser. B: Geol., Khim. Biol. Nauki* **1988**, 47.

(7) (a) Hyde, B. G.; Andersson, S. *Inorganic Crystal Structures*; Wiley-Interscience: New York, 1989. (b) Hyde, B. G.; O'Keeffe, M.; Lyttle, W. M.; Brese, N. E. *Acta Chem. Scand.* **1992**, *46*, 216.

(8) Hulliger, F. *Struct. Bonding* **1968**, *4*, 83.

(9) Jeitschko, W. *Acta Crystallogr. Sect. B* **1968**, *B24*, 930.

(10) Flahaut, J.; Thévet, F. *J. Solid State Chem.* **1979**, *32*, 365.

0020-1669/95/1334-2962$09.00/0

Exhibit C

J. Am. Chem. Soc., **119** (52), 12824 -12830, 1997. 10.1021/ja9718681 S0002-7863(97)01868-4

Novel Quaternary Metal-Rich Phosphides: Stabilization by Differential Fractional Site Occupancies and Polar Intermetallic Bonding

Holger Kleinke† and Hugo F. Franzen*

Contribution from the Ames Laboratory, DOE-Iowa State University, Ames, Iowa 50011

Received June 6, 1997⊗

Abstract:

The new phosphide $Hf_5Nb_5Ni_3P_5$ has been prepared by arc-melting of a pressed stoichiometric mixture of HfP, Nb, and Ni. Single crystals suitable for the structure determination were obtained after annealing in an induction furnace at 1350 °C. $Hf_5Nb_5Ni_3P_5$ crystallizes in the hexagonal space group $P\bar{6}2m$ (No. 189). The early transition metal atoms Hf and Nb are found on three crystallographically different sites, with refined occupancies of 100% Hf for the M1, 59.5(4)% Hf and 40.5(4)% Nb for the M2, and 13.1(6)% Hf and 86.9(6)% Nb for the M3 site. Small variations of the Hf to Nb ratio are possible, occurring with significantly different lattice parameters. The early transition elements form a three-dimensional framework with numerous M-M (M = Hf, Nb) interactions, including Ni and P in its trigonal prismatic voids. The differential fractional site occupancies can be understood on the basis of the different preferences of Hf and Nb to form M-M, M-Ni, and M-P bonds. The metallic character is confirmed by the Pauli paramagnetism experimentally obtained.

Exhibit D

American Mineralogist, Volume 83, pages 133–140, 1998

High form of pentlandite and its thermal stability

ASAHIKO SUGAKI[1] AND ARASHI KITAKAZE[2]

[1]4-30-503, Kadan, Aoba-ku, Sendai 980, Japan
[2]Institute of Mineralogy, Petrology and Economic Geology, Faculty of Science, Tohoku University, Sendai 980-77, Japan

ABSTRACT

The high-temperature form of pentlandite ($Fe_{4.5}Ni_{4.5}S_8$) was found to be stable between 584 ± 3 and 865 ± 3 °C, breaking down into monosulfide solid solution and liquid at the later temperature. The phase is unquenchable and always displays the X-ray pattern of pentlandite (low form) at room temperature. High-temperature X-ray diffraction demonstrated that the high form has a primitive cubic cell with a = 5.189 Å (620 °C) corresponding to $a/2$ of pentlandite. The high-low inversion is reversible, accompanied by a large latent heat. It is thought to be order-disorder in character. The transition temperature falls with decreasing S content. The high form of pentlandite has a limited solid solution from $Fe_{5.07}Ni_{3.93}S_{7.85}$ to $Fe_{3.61}Ni_{5.39}S_{7.85}$ at 850 °C. However its solid solution extends rapidly toward $Ni_{3\pm x}S_2$ in the Ni-S join with decreasing temperature. High-form pentlandite with Fe = Ni in atomic percent crystallizes first by a pseudoperitectic reaction between monosulfide solid solution and liquid. The high form (Fe = Ni) crystallized from the liquid always has the metal-rich (S-poor) composition in the solid solution at each temperature and coexists with taenite γ (Fe,Ni) below 746 ± 3 °C. This metal-rich high-form $Fe_{4.5}Ni_{4.5}S_{7.4}$ breaks down into pentlandite and γ (Fe,Ni) at 584 ± 3 °C (pseudoeutectoid).

These results suggest that in geological processes, such as the formation of Ni-Cu ore deposits, pentlandite can crystallize as the high form from liquid (sulfide magma) at the comparatively high temperatures around 800 °C.

INTRODUCTION

Kullerud (1962, 1963a) reported that pentlandite $Fe_{4.5}Ni_{4.5}S_8$ is present as a stable phase below 610 °C, but breaks down into a mixture of $Ni_{3\pm x}S_2$ and pyrrhotite (monosulfide solid solution) at this temperature or above. However Sugaki et al. (1982) and Sugaki and Kitakaze (1992) found instead that pentlandite transforms into a high form at 610 °C that is stable up to 865 °C. The existence of a high-form pentlandite as the stable phase required the reexamination and revision of the Fe-Ni-S phase diagrams above 600 °C, especially in the central portion of the system, given by Kullerud (1963b), Kullerud et al. (1969), and Hsieh et al. (1982). Sugaki et al. (1984) found that high-form pentlandite shows continuous solid solution from $Fe_{4.97}Ni_{4.03}S_{7.85}$ and $Fe_{5.37}Ni_{3.63}S_{7.89}$ to $Ni_{3\pm x}S_2$ (Rosenqvist 1954; Kullerud and Yund 1962) in the Ni-S join at 800 and 650 °C, respectively.

In this paper, we present new experimental data on the thermal stability of the low form of pentlandite together with its phase transition and the phase relations of high-form pentlandite in the Fe-Ni-S system. Chemical compositions and crystal data for minerals and phases in the Fe-Ni-S ternary synthesized here are given in Table 1. Phase equilibria in the Fe-Ni-S system at temperatures from 600 to 850 °C will be reported in a subsequent paper.

HIGH-TEMPERATURE SYNTHESES

Evacuated silica glass-tube method

Fe (99.999%) and Ni (99.999%) from Johnson Matthey Co., Ltd., and S (99.99%) from Kanto Chemical Co., Ltd., were used as starting materials. The metals and S were precisely weighed in the proportion to the compositions of the pentlandite solid solution (SS), and then they were sealed in the silica tube under vacuum of 1.33×10^{-1} Pa (10^{-3} Torr). The sealed tubes with the charge were kept at 800 °C for 7 d after preheating at 400 to 500 °C for 3 d. The product was homogenized by grinding, resealed in an evacuated silica tube, and reheated at 650, 800, or 850 °C for at least 10 d. The tube was then cooled rapidly in ice water. The final products were aggregates of fine anhedral grains of pentlandite, 10 to 50 μm in size. Its homogeneity was examined by reflected-light-microscopy, X-ray diffraction, and microprobe analysis, and found to be a monophase.

Vapor transportation method

Approximately 100 mg of powdered pentlandite ($Fe_{4.50}Ni_{4.50}S_{7.80}$), synthesized as above, and 0.5 mg of iodine were sealed together in an evacuated silica tube, heated at 770 °C for 7 d in a vertical electric furnace, and then cooled to room temperature. Euhedral pentlandite corresponding to the high form had recrystallized as a fine-grained aggregate

0003–004X/98/0102–0133$05.00

TABLE 1. Chemical compositions and crystallographic data of minerals and phases in this study

Mineral names	Abbrev.	Composition	Structure type (cell edges in Å)	References
Pyrrhotite	po	$Fe_{1-x}S$	Hexagonal 1C a = 3.45, c = 5.75	Nakazawa and Morimoto (1971)
Pentlandite	pn	$(Fe,Ni)_9S_8$	Cubic Fm3m a = 10.03	Rajamani and Prewitt (1973)
High-form pentlandite	hpn	$(Fe,Ni)_9S_8$	Cubic pc a = 5.189 (at 620 °C)	This study
Monosulfide solid solution	mss	$(Fe,Ni)_{1-x}S$	Hexagonal a = 3.45, c = 5.6	Craig and Scott (1974)
Vaesite	vs	NiS_2	Cubic Pa3 a = 5.670	Kerr (1945)
Godlevskite	gs	Ni_7S_6	Orthorhombic C222 a = 9.336, b = 11.218, c = 9.430	Fleet (1987)
Heazlewoodite	hz	Ni_3S_2	Hexagonal R32 a = 5.747, c = 7.135	Fleet (1977)
High-form heazlewoodite		$Ni_{3\pm x}S_2$	Cubic Fm3m a = 5.22 (at 640 °C)	Liné and Huber (1963)
Taenite	tn	γ(Fe,Ni)	Cubic Fm3m a = 7.146	Ramsden and Cameron (1966)
Iron	ir	αFe	Cubic a = 2.8664	Ramsden and Cameron (1966)

near the top of the tube. The crystal faces were principally well-developed (111) and (100) forms.

Flux method

About 200 mg of NaCl-KCl salts with 1:1 molecular ratio and 200 mg of powdered pentlandite ($Fe_{4.50}Ni_{4.50}S_{7.80}$) synthesized by the evacuated silica tube method were sealed in a silica glass tube under vacuum of 1.33×10^{-1} Pa. The tube was kept at 800 °C for 7 d. The result was aggregates of euhedral high-form pentlandite, similar to those formed by the vapor transportation method.

EXPERIMENTAL PROCEDURES AND RESULTS

Microscopic examinations

Pentlandite of composition $Fe_{4.50}Ni_{4.50}S_{7.80}$ synthesized at 800 °C by the evacuated silica glass tube method is yellowish gray in color with a metallic luster at room temperature. Under the reflected light microscope, it appears light creamy white in color and has a distinct octahedral cleavage. It is isotropic. The values of its reflectance in the air are 436 nm: 38.4 ± 0.2%, 497 nm: 46.0 ± 0.2%, 546 nm: 49.1 ± 0.2%, 586 nm: 51.4 ± 0.2%, and 648 nm: 53.9 ± 0.2%. These optical properties are in accord with those found previously for pentlandite (Picot and Johan 1982; Criddle and Stanley 1986).

Fine-grained crystals of heazlewoodite, godlevskite (low form Ni_7S_6), and taenite γ (Fe,Ni) appeared as quench products in Ni-rich high-form pentlandite SS and $(Ni,Fe)_{3\pm x}S_2$, but high-form pentlandite samples with compositions around Ni/Fe = 1 and more than ~46 at% S were almost homogeneous after quenching.

Fine-grained euhedral crystals obtained both by vapor transportation and flux were examined by scanning electron microscope. The SEM photomicrographs of euhedral high-form pentlandite are shown in Figure 1.

Electron probe microanalysis

Electron probe microanalysis (EPMA) was used to ascertain the homogeneity of the synthetic pentlandites and analyze their chemical compositions. Synthetic FeS was used as a standard for Fe and S, whereas NiS was the standard for Ni. The Bence and Albee (1968) method was used for correcting the X-ray intensity ratio. Compositions of crystals grown at 800 °C in flux are in the range of $Fe_{4.25-5.03}Ni_{3.97-4.75}S_{7.89-8.08}$ (Table 2[1]), and generally are very close to that of the stoichiometric pentlandite.

Compositions of crystals precipitated at 770 °C by vapor transportation are in the range of $Fe_{3.09-3.87}Ni_{5.13-5.91}S_{7.19-7.70}$ (Table 3[1]). All the compositions correspond to those of Ni-rich high-form pentlandite SS. For the evacuated silica tube method at 850 °C, the compositions of the monophase products with Fe = Ni (in atomic percent) were Fe: 26.47, Ni: 26.47, S: 47.06 ($Fe_{4.50}Ni_{4.50}S_{8.00}$) and ($Fe_{4.50}Ni_{4.50}S_{8.00}$) and Fe: 26.79, Ni: 26.79, S: 46.42 ($Fe_{4.50}Ni_{4.50}S_{7.80}$) (Table 4[1]). High-form pentlandite (with only monosulfide SS present or monosulfide SS and liquid present) is present as a SS of the limited range from $Fe_{5.06}Ni_{3.94}S_{7.85}$ to $Fe_{3.61}Ni_{5.39}S_{7.85}$ including $Fe_{4.50}Ni_{4.50}S_{8.00}$ (Table 5[1]). However the high-form pentlandite SS extends rapidly toward $Ni_{3\pm x}S_2$ in the Ni-S join with decreasing temperature and reaches the join as a continuous SS below 806 °C at which point $Ni_{3\pm x}S_2$ (Kullerud and Yund 1962) or Ni_4S_3 (Lin et al. 1978) appear. From the monophase data obtained by the silica tube synthesis, we find that the high-form pentlandite SS forms a continuous SS with $Ni_{3\pm x}S_2$ (or Ni_4S_3) at 800 and 650 °C.

High-temperature X-ray diffraction

Because the high form of pentlandite and its SS are unquenchable, a high-temperature heating unit was used to examine one sample with composition $Fe_{4.50}Ni_{4.50}S_{7.80}$ synthesized by the evacuated silica tube method at 800 °C. Approximately 30 mg of the powdered sample was

[1] For a copy of Tables 2, 3, 4, 5, 7, 8, and 9, Document AM-98-001, contact the Business Office of the Mineralogical Society of America (see inside front cover of recent issue) for price information. Deposit items may also be available on the American Mineralogist web site (see inside back cover for a current web address).

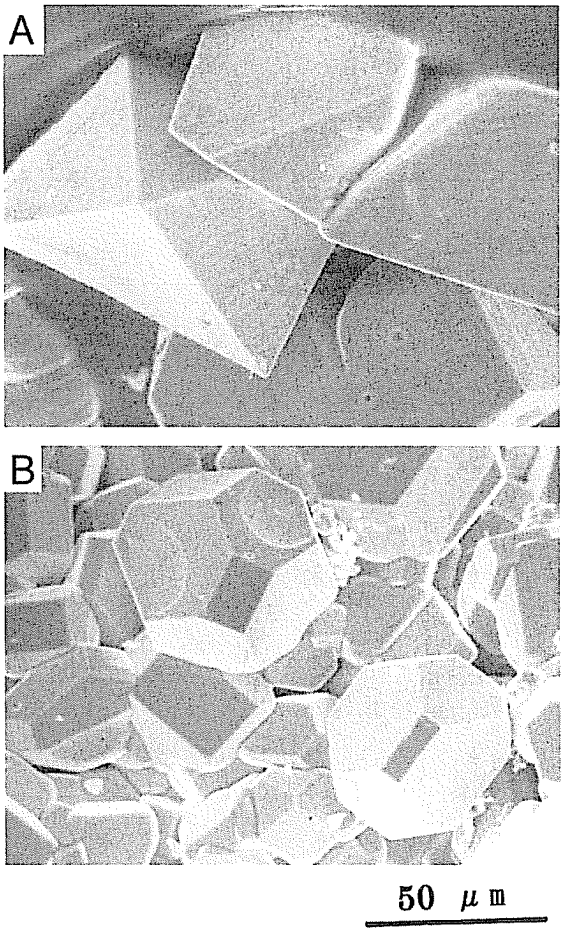

FIGURE 1. Photomicrographs of high-form pentlandite crystals by scanning electron microscope. **A** = Euhedral crystals of high-form pentlandite synthesized by the I_2 vapor transportation method at 770 °C. **B** = High-form pentlandite crystals synthesized by the KCl-NaCl flux method at 800 °C.

mounted on a gold sample holder. The surface of the sample was coated with a gold film by a vacuum evaporator to keep the surface of the sample flat up to 700 °C and to prevent oxidation. The heating unit was evacuated with a rotary vacuum pump and then filled up with a purified nitrogen gas. The X-ray powder patterns for the pentlandite sample were taken using Cu$K\alpha$ (35 kV, 15 mA) from 25 to 620 °C in a slow flow of nitrogen gas. Also, the gold coating was used as a standard for correction of the reflection peaks in the powder pattern at high temperature, by using its expansion coefficient. Metallic silicon was also used as an internal standard but possibly reacted with the sample at high temperature. Temperature was measured with a Pt-Pt-Rh (13%) thermocouple inserted into a small well of the sample holder. The temperature difference between the holder well and sample was within ±2 °C at 600 °C. The temperature during the measurement was regulated to within ±1 °C.

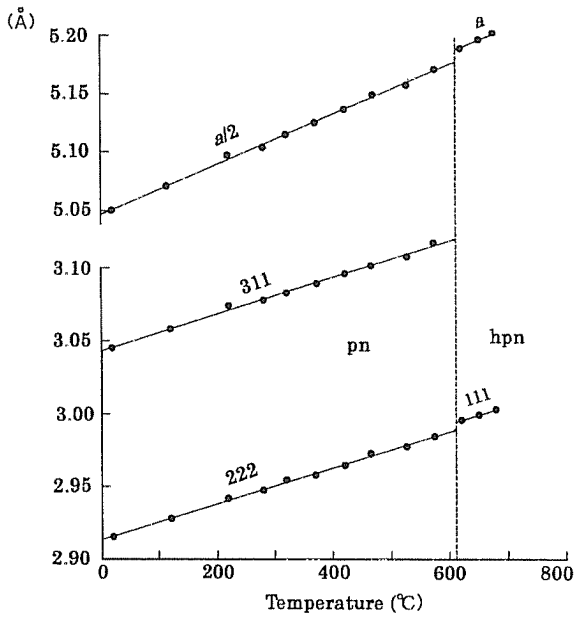

FIGURE 2. The cubic cell edges and spacings of d_{311} and d_{222} of pentlandite ($Fe_{4.50}Ni_{4.50}S_{7.80}$) and d_{111} of its high form vs. the temperatures. Abbreviations: See Table 1.

Values of the cell edge and spacings d_{311} and d_{222} vs. the temperature (Fig. 2) increase linearly with increasing temperature. The linear thermal expansion coefficient of pentlandite ($Fe_{4.50}Ni_{4.50}S_{7.80}$) calculated using the cell edges is 13.4 × 10^{-5} °C^{-1} (25 to 580 °C). This value agrees very well with 13.5 × 10^{-5} °C^{-1} (25 to 608 °C) calculated by us using the data on thermal change of the cell edge for synthetic pentlandite ($Fe_{4.5}Ni_{4.5}S_{7.8}$) by Morimoto and Kullerud (1964), but larger than 11.1 × 10^{-5} °C^{-1} (24 to 200 °C) for pentlandite from Frood, Sudbury, sample studied by Rajamani and Prewitt (1975).

The powder patterns above 620 °C differ remarkably from those of the same sample below 580 °C (Fig. 3).

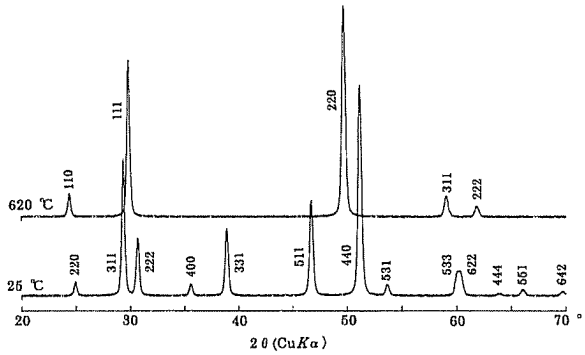

FIGURE 3. X-ray powder diffraction patterns of synthetic pentlandite and high-form pentlandite with $Fe_{4.50}Ni_{4.50}S_{7.80}$ at 25 and 620 °C, respectively.

TABLE 6. X-ray powder diffraction data for synthetic pentlandite ($Fe_{4.50}Ni_{4.50}S_{7.80}$) at 25, 280, and 580 °C and for high-form pentlandite at 620 °C

	Pentlandite ($Fe_{4.50}Ni_{4.50})_8S_{7.80}$							High-form pentlandite	
	25 °C		280 °C		580 °C			620 °C	
hkl	I	d(obs)	I	d(obs)	I	d(obs)	*hkl*	I	d(obs)
111	24	5.84	20	5.89	25	5.97			
200	6	5.051	5	5.104	5	5.172			
220	6	3.571	5	3.607	5	3.656	110	10	3.649
311	60	3.045	40	3.077	45	3.119			
222	25	2.916	15	2.945	20	2.988	111	70	2.996
400	5	2.524	2	2.551	2	2.584			
331	30	2.317	15	2.342	10	2.374			
511	44	1.945	30	1.966	25	1.990			
440	100	1.786	100	1.804	100	1.825	220	100	1.835
531	5	1.708	2	1.728	2	1.749			
533	10	1.541	5	1.557	5	1.577			
622	9	1.533	7	1.538	7	1.558	311	10	1.564
444	1	1.457	2	1.473	2	1.493	222	5	1.500
551	3	1.414	2	1.429	2	1.449			
642	2	1.349	2	1.364	1	1.382			
a		10.100(1)		10.206(2)		10.344(2)			5.189(3) Å

Note: Radiation = Cu$K\alpha$ (35 kV, 15 mA). Scanning speed of goniometer = 1°/min.

The reflections of type $hkl \neq 2n$ below 580 °C disappear at 620 °C, but reflections of type $hkl = 2n$ remain. Because all the reflections at 620 °C correspond to those of the even number indices of pentlandite below 580 °C, they were indexed in terms of a cubic cell with $a/2$ of pentlandite below 580 °C (Table 6). The change is reversible. At 620 °C, reflections that indicate the appearance of other phases, for instance monosulfide SS, were not found.

X-ray diffraction data for single crystals of high-form pentlandite synthesized by both the vapor transportation and flux methods at 770 and 800 °C, respectively, were obtained using a precession camera with a platinum wire furnace. A single crystal of pentlandite was placed inside a 0.5 mm diameter silica glass capillary and fixed with a silica glass fiber inserted into the tube. The capillary was evacuated and sealed. The sample was equilibrated at the desired temperature for one day, then an exposure was taken over 2 d. Temperature was measured with a chromel-alumel thermocouple set 3 mm from the specimen tube and controlled continuously within ±1 °C by a regulator. The temperature difference between specimen and the head of the thermocouple was within ±5 °C at 600 °C.

A representative [110] precession photograph of synthetic pentlandite ($Fe_{4.56}Ni_{4.44}S_{7.95}$) at room temperature (25 °C) is shown in Figure 4A. Diffraction patterns taken at 200, 400, and 580 °C are similar. However the precession photograph at 620 °C (Fig. 4B), differs markedly. Reflections of the odd number indices seen in the photographs below 580 °C disappear at 620 °C, but those of the even number indices remain at high temperature. These reflections at 620 °C are indexed as 110, 111, and 220 for the cubic cell with a cell edge that is half of the low form of pentlandite as seen in the photograph. The cubic cell edge of the single crystal at 620 °C is $a = 5.19$ Å. This value of the cell edge is in good agreement with that obtained from the powder data at 620 °C. The diffraction pattern for the single crystal, cooled down to room temperature from 620 °C, returned to the original form (Fig. 4A).

Similar results were obtained for the high-temperature powder and single-crystal patterns of natural pentlandite ($Fe_{4.11}Ni_{4.85}Co_{0.08}S_{7.96}$) from Copper Cliff, Sudbury.

It is clear that a reversible phase transition occurs at a temperature between 580 and 620 °C in which the size of unit-cell edge doubles. No compositional change at the transition is found, and it is possible that this transition is an order-disorder inversion from the supercell (low form) to the subcell.

Differential thermal analysis

To ascertain the thermal behavior and stability of pentlandite, differential thermal analysis (DTA) was performed using an evacuated silica glass tube as a reaction vessel. A sample synthesized at 800 °C by the evacuated silica tube method was used. Alpha alumina was used as a reference material. Chromel-alumel thermocouples were used for both the differential and sample temperatures.

DTA was normally carried out at fixed heating rates of 5 and 10 °C/min from room temperature to 1000 °C or above. Sometimes the DTA was performed at a slower heating rate of 1 and 2 °C/min from 550 to 1000 °C to pinpoint the temperatures of the thermal reactions more accurately. The sample heated up to above 1000 °C was also cooled in the furnace, and the DTA curve on the cooling was obtained again at the spontaneous cooling rate of the furnace. Temperatures were calibrated using the melting points of high-purity tin (231.97 °C), zinc (419.6 °C), aluminum (660.4 °C), and silver (961.9 °C).

Two strong endothermic reactions beginning at 610 and 865 °C are seen during heating (Fig. 5, curve A). The

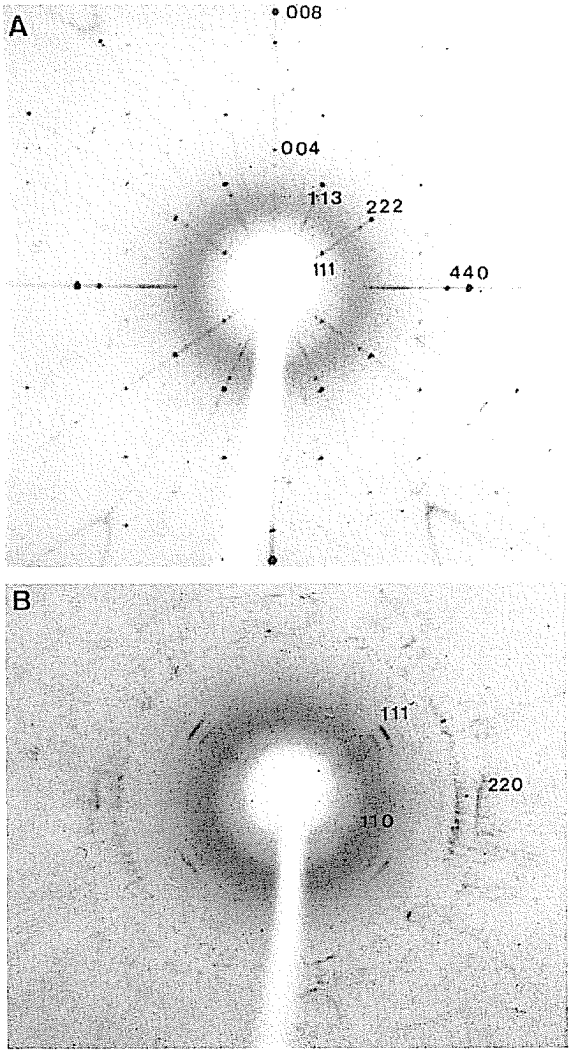

FIGURE 4. Two [110] precession photographs for a single crystal of synthetic low- and high-form pentlandites with $Fe_{4.56}Ni_{4.44}S_{7.95}$ at 25 and 620 °C, respectively. **A** = 25 °C; **B** = 620 °C.

later reaction still continues with increasing temperature and finishes at 952 °C. These reactions also appear as the exothermic peaks during cooling (curve B). The continuous reaction from 865 to 952 °C in the heating curve (Fig. 5A) is clearly seen in the cooling curve (Fig. 5B).

From microscope observations, EPMA, X-ray diffraction, and DTA, we conclude that the feature at 610 °C is due to a high-low inversion, and the feature at 865 °C arises from the breakdown of high-form pentlandite into monosulfide SS and liquid. The continuous reaction between 865 and 952 °C corresponds to successive melting of monosulfide SS, which is a breakdown product of high-form pentlandite at 865 °C. Finally the remnant monosulfide SS melts at 952 ± 5 °C.

The transition temperature of pentlandite with Fe = Ni

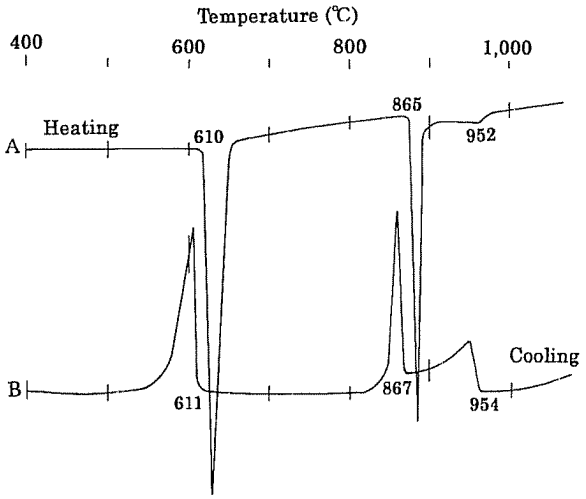

FIGURE 5. DTA Curves of synthetic pentlandite (and high-form pentlandite) with $Fe_{4.50}Ni_{4.50}S_{7.80}$. (**A**) Heating curve of 10 °C/min. (**B**) Cooling cure.

(in at%) at around 600 °C depends on composition, especially S content. The transition temperature of $Fe_{4.50}Ni_{4.50}S_{7.90}$ with monosulfide SS is 615 ± 3 °C, a slightly higher temperature than that of $Fe_{4.50}Ni_{4.50}S_{7.80}$. However the transition of metal-rich (S-poor) pentiandite ($Fe_{4.50}Ni_{4.50}S_{7.70}$) occurs over a temperature range from 586 to 604 °C, as is discussed below.

HIGH-FORM PENTLANDITE PHASE RELATIONS

Isothermal phase relations at 850 °C

Phase relations of high-form pentlandite in the metal-rich portion of the Fe-Ni-S system (Fig. 6) were determined from optical properties, X-ray powder diffraction data, and EPMA (Table 8[1]). High-form pentlandite appears as a stable phase at 850 °C with a limited SS from $Fe_{5.07}Ni_{3.93}S_{7.85}$ to $Fe_{3.61}Ni_{5.39}S_{7.85}$ including stoichiometric $Fe_{4.50}Ni_{4.50}S_{8.00}$ and coexists with monosulfide SS in the S-rich side and liquid in the metal-rich side. High-form pentlandite samples of both the Fe- and Ni-rich ends of the SS coexist with each monosulfide SS and liquid as univariant assemblages. However high-form pentlandite cannot coexist with taenite γ (Fe,Ni) at 850 °C because of existence of the extensive liquid field.

Thermal stabilities of pentlandites

A phase diagram of the S compositions from 35 to 52 at% with Fe = Ni vs. the temperatures was constructed (Fig. 7) using the equilibrium experiment data (Table 9[1]) and the DTA data (Table 10). Both high- and low-form samples with Fe = Ni show limited SS across a restricted S-composition range. A small two-phase field containing both forms of pentlandite is found between 584 and 615 °C. Pentlandite of composition $Fe_{4.50}Ni_{4.50}S_{7.90}$ coexists with monosulfide SS and inverts to high-form pentlandite at 615 ± 3 °C. However the transition temperature falls

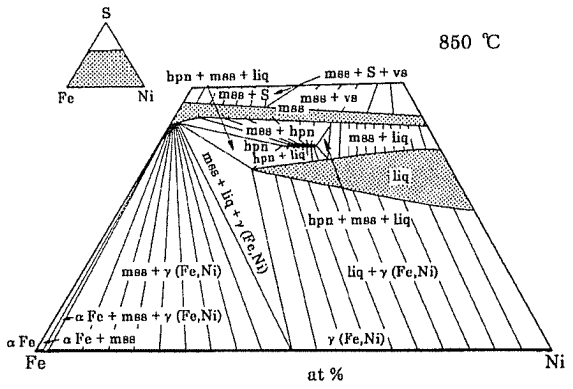

FIGURE 6. The phase relations of the metal-rich portion in the Fe-Ni-S system at 850 °C. Abbreviations: See Table 1; liq = liquid.

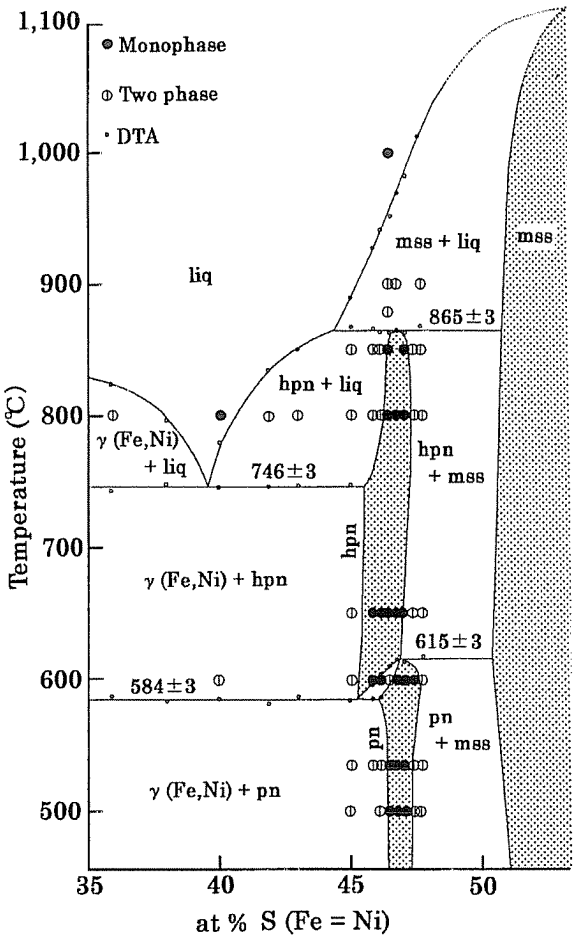

FIGURE 7. The phase diagram of the sulfur composition with Fe = Ni vs. the temperature. The boundary of monosulfide SS below 600 °C referred to Naldrett et al. (1967). Abbreviations: See Table 1; liq = liquid

from 615 to 584 °C with decreasing the S content. This transition is reversible.

High-form pentlandite of a metal-rich composition generally shows fine-grained crystals of γ (Fe,Ni) when quenched. In these circumstances, we were able to distinguish the high-form pentlandite from the low form under the microscope and by EPMA. However, as seen in S-rich high-form pentlandite, when γ (Fe,Ni) did not appear by quenching, it proved difficult to distinguish both the two phases after quench.

High-form pentlandite ($Fe_{4.50}Ni_{4.50}S_{7.90}$) is stable up to 865 ± 3 °C, when it breaks down into monosulfide SS and liquid. The products of the breakdown of high-form pentlandite of composition $Fe_{4.50}Ni_{4.50}S_{7.80}$ (Fe = Ni: 26.79 at% and S: 46.42 at%) at 880 °C are shown in Figure 8 (and Table 9[1]). At 1000 °C, the entire charge is similar in appearance to the liquid patch shown in Figure 8. A pseudoeutectic point exists at 746 ± 3 °C and 39.3 at% S in the metal-rich portion of the binary. The most metal-rich high-form pentlandite SS (Fe = Ni) coexisting with γ (Fe,Ni) breaks down into pentlandite (low form) and γ (Fe,Ni) in the pseudoeutectoid reaction at 584 ± 3 °C and 45.2 at% S (Fig. 7).

Discussion

As mentioned above, the thermal stability range of pentlandite including its high form in fact extends up to 865 °C, approximately 255 °C higher than 610 °C suggested by Kullerud (1962, 1963a). The phase diagram of the Fe-Ni-S system at temperatures above 600 °C by Kullerud (1963b), Kullerud et al. (1969), and Hsieh et al. (1982) should now be re-appraised because the high form of pentlandite was not previously identified, although they did report a ternary phase $(Ni,Fe)_{3\pm x}S_2$ near the Ni-S join at 860 (Kullerud 1963b) and 850 °C (Hsieh et al. 1982). The high form of pentlandite has a SS with a limited range from $Fe_{5.07}Ni_{3.93}S_{7.85}$ to $Fe_{3.61}Ni_{5.39}S_{7.85}$ including $Fe_{4.50}Ni_{4.50}S_{8.00}$ at 850 °C (Fig. 6).

We have found that the high-form pentlandite SS extends rapidly to the Ni-rich direction with decreasing temperature, and continues with $Ni_{3\pm x}S_2$ below 806 °C, the breakdown (or incongruent melting) temperature of $Ni_{3\pm x}S_2$ (Kullerud and Yund 1962). The compositional data of high-form pentlandite SS and $(Fe,Ni)_{3\pm x}S_2$ synthesized at 800 °C indicate the existence of a continuous SS between high-form pentlandite and $Ni_{3\pm x}S_2$. The SS is maintained at 650 °C. These results are in agreement with other recent findings: Fedorova and Sinyakova (1993) found high-form pentlandite SS (heazlewoodite SS in their terminology) at 820 °C. Karup-Møller and Makovicky (1995) also reported the existence of a continuously extensive SS, $(Fe,Ni)_{3\pm x}S_2$, between high-form pentlandite and $Ni_{3\pm x}S_2$ at 725 °C.

The crystallization of the high form of pentlandite with Fe = Ni may now be understood from Figure 7 as follows: The high form crystallizes first by a pseudoperitectic reaction between monosulfide SS and liquid at 865 ± 3 °C and successively precipitates directly from the liquid

TABLE 10. Temperatures of the phase reactions obtained by DTA in the composition range from 35 to 48 at% S of the $(Fe_{0.5}Ni_{0.5})$–S join in the Fe-Ni-S system

	at%			°C				
Run no	Fe	Ni	S	T_1	T_2	T_3	T_4	T_5
FNS3876	26.16	26.16	47.68		618		868	1012
FNS3871	26.47	26.47	47.06		613		863	982
FNS4002	26.63	26.63	46.74		615		865	970
FNS3869	26.79	26.79	46.42		600–610		865	952
FNS4001	26.95	26.95	46.10		586–604		864	941
FNS3873	27.11	27.11	45.78	584	595		866	928
FNS3936	27.50	27.50	45.00	583		747	868	890
FNS3937	28.50	28.50	43.00	587		747		851
FNS3960	29.03	29.03	41.94	581		746		835
FNS3980	30.00	30.00	40.00	585		745		780
FNS3959	31.03	31.03	37.94	584		749		797
FNS3958	32.14	32.14	35.72	587		743		825
				584 ± 3		746 ± 3	865 ± 3	

Note: T_1 = Pseudoeutectoid; T_2 = Inversion between pentlandite and high-form pentlandite; T_3 = Pseudoeutectic; T_4 = Breakdown (incongruent melting) of high-form pentlandite; T_5 = Liquidus (completely melting).

with decreasing temperature down to 746 ± 3 °C, corresponding to a pseudoeutectic in the ternary. This pseudoeutectic continues to a eutectic point at 637 °C and 33 at% S in the Ni-S join (Singleton et al. 1991). The high-form pentlandite crystallized from liquid below 865 °C has the metal-rich composition at each temperature and always coexists with γ (Fe,Ni) below 746 °C in the equilibrium state. This metal-rich high-form pentlandite ($Fe_{4.5}Ni_{4.5}S_{7.4}$) breaks down into pentlandite (low form) and γ (Fe,Ni) as a pseudoeutectoid reaction at 584 ± 3 °C and 45.2 at% S. The pseudoeutectoid continues to a ternary eutectoid point at 470 °C and approximately 13 Fe, 49 Ni, and 38 S in atomic percentages near the Ni-S boundary in the Fe-Ni-S system (Fedorova and Sinyakova 1993). On the other hand, high-form pentlandite ($Fe_{4.50}Ni_{4.50}S_{7.90}$) coexisting with monosulfide SS inverts into pentlandite of the same composition at 615 ± 3 °C.

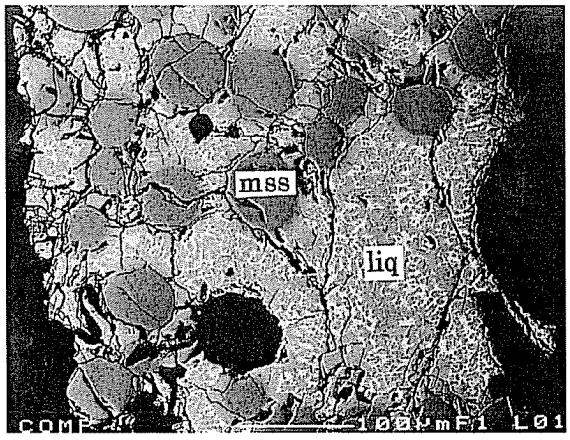

FIGURE 8. Back-scattered electron images by EPMA for the breakdown products of high-form pentlandite ($Fe_{4.50}Ni_{4.50}S_{7.80}$) at 880 °C into monosulfide SS and liquid (liq), which is a mixture of pentlandite (dark gray) and γ (Fe,Ni) (light gray) as quenched products. Abbreviations: See Table 1.

This inversion temperature falls continuously from 615 to 584 ± 3 °C with decreasing S content. Because the inversion passes through a two-phase field of coexisting high- and low-form pentlandites within the loop, the inversion should exist over some temperature range (maximum 20 °C in Fig. 7). However this temperature range was difficult to detect precisely by DTA.

The existence of high-form pentlandite as a stable phase up to 865 °C (the breakdown temperature of high-form pentlandite) shows that the previous inference of pentlandite genesis by Kullerud (1962, 1963a) are probably incorrect. High-form pentlandite with Fe = Ni can crystallize from liquid at temperatures between 865 and 746 °C (Fig. 7). The existence of a stable high-form pentlandite phase at high temperature is supported by the observation of genesis of Ni-Cu ores with pentlandite crystallized directly from sulfide magma (Lindgren 1933; Bateman 1952).

When pentlandite inverts into high-form pentlandite, a large latent heat anomaly is displayed in the DTA curve (Fig. 5). The enthalpy appears to be as much as or nearly equal to that of the latent heats of melting and breakdown reactions. Kullerud (1962), therefore, believed that the strong peak at 610 °C could not be explained as the result of a polymorphic inversion but rather indicates the breakdown of the pentlandite phase. Our experiments, however, refute this interpretation. Such a large latent heat of inversion is a rare case in sulfide and is thought to be caused by a peculiarity of the pentlandite crystal structure, which is characterized by alternating the arrangement of subcells with eight tetrahedrally coordinated cations and with an octahedrally coordinated cation (Lindqvist et al. 1936; Rajamani and Prewitt 1973). Apparently, transformation of such a distinctively ordered structure into a disordered primitive cubic cell can cause a large heat anomaly.

ACKNOWLEDGMENTS

The authors are grateful for assistance by T. Hayashi in the experiments. We thank Simon A.T. Redfern for his helpful suggestions and reviews of the manuscript, and two anonymous reviewers for their critical comments.

References cited

Bateman, A.M. (1952) Economic mineral deposits, 875 p. Wiley, London.

Bence, A.E. and Albee, A.L. (1968) Empirical correction factors for the electron microanalysis of silicate and oxides. Journal of Geology, 76, 382–403.

Craig, J.R. and Scott, S.D. (1974) Sulfide phase equilibria. Mineralogical Society of America Short Course Notes, CS1–110.

Criddle, A.J. and Stanley, C.J. (1986) The quantitative data file for ore minerals. The Commission on Ore Microscopy of the International Mineralogical Association, 275 p. British Museum, London.

Fedorova, Z.N. and Sinyakova, E.F. (1993) Experimental investigation of physicochemical conditions of pentlandite formation. Geologiya i Geofizika, 34, 84–92 (in Russian).

Fleet, M.E. (1977) The crystal structure of heazlewoodite and metallic bonds in sulfide minerals. American Mineralogist, 62, 341–345.

———(1987) Structure of godlevskite, Ni_9S_8. Acta crystallographica, C43, 2255–2257.

Hsieh, K.-C., Chang, Y.A., and Zhong, T. (1982) The Fe-Ni-S system above 700 °C. Bulletin of Alloy Phase Diagrams, 3, 165–172.

Karup-Møller, S. and Makovicky, E. (1995) The phase system Fe-Ni-S at 725 °C. Neues Jahrbruch for Mineralogie Monatshefte, 1–10.

Kerr, P.F. (1945) Cattierite and vaesite: New Co-Ni minerals from the Belgian Congo. American Mineralogist, 30, 483–497.

Kullerud, G. (1962) The Fe-Ni-S system. Carnegie Institute of Washington Year Book, 61, 144–150.

———(1963a) Thermal stability of pentlandite. Canadian Mineralogist, 7, 353–366.

———(1963b) The Fe-Ni-S system. Carnegie Institute of Washington Year Book, 62, 175–189.

Kullerud, G. and Yund, R.A. (1962) The Ni-S system and related minerals. Journal of Petrology, 3, 126–175.

Kullerud, G., Yund, R.A., and Moh, G.H. (1969) Phase relations in the Cu-Fe-S, Cu-Ni-S, and Fe-Ni-S systems. In H.D.B. Wilson, Ed., Magmatic ore deposits, p. 323–343. Economic Geology Monograph 4.

Lin, R.Y., Hu, D.C., and Change, Y.A. (1978) Thermodynamics and phase relationships of transition metal-sulfur system: II. The nickel-sulfur system. Metallurgical Transactions B, 9B, 531–538.

Lindgren, W. (1933) Mineral deposits (4th edition), 930 p. McGraw-Hill Book Co., New York.

Lindqvist, M., Lundqvist, D., and Westgren, A. (1936) The crystal structure of Co_9S_8 and of pentlandite $(Ni,Fe)_9S_8$. Kemisk Tidskrift, 48, 156–160.

Liné, G. and Huber, M. (1963) Étude radiocristallographique à haute température de Ia phase non stoechiométrique $Ni_{1-x}S_2$. Comptes Rendus de l'Académie des Sciences, 256, 3118–3120.

Morimoto, N. and Kullerud, G. (1964) Pentlandite thermal expansion. Carnegie Institute of Washington Year Book, 63, 204–205.

Nakazawa, H. and Morimoto, N. (1971) Phase relations and super-structures of pyrrhotite, $Fe_{1-x}S$. Material Research Bulletin, 6, 345–358.

Naldrett, A.J., Craig, J.R., and Kullerud, G. (1967) The central portion of the Fe-Ni-S system and its bearing on pentlandite exsolution in iron-nickel sulfide ores. Economic Geology, 62, 826–847.

Picot, P. and Johan, Z. (1982) Atlas of ore minerals, p. 293–294. Elsevier, Amsterdam.

Rajamani, V. and Prewitt, C.T. (1973) Crystal chemistry of natural pentlandites. Canadian Mineralogist, 12, 178–187.

Rajamani, V. and Prewitt, C.T. (1975) Thermal expansion of the pentlandite structure. American Mineralogist, 60, 39–48.

Ramsden, A.R. and Cameron, E.N. (1966) Kamacite and taenite superstructures and a metastable tetragonal phase in iron meteorites. American Mineralogist, 51, 37–55.

Rosenqvist, T. (1954) A thermodynamic study of the iron, cobalt, and nickel sulfides. Journal of the Iron and Steel Institute, 176, 37–57.

Singleton, S., Nash, P., and Lee, K.J. (1991) Ni-S. In T.B. Massalski, J.L. Munay, L.H. Bennet, and H. Baker, Eds., Binary alloy phase diagram, vol. 1, p. 2850–2853. American Society for Metals, Metal Park, Ohio.

Sugaki, A. and Kitakaze, A. (1992) Phase transition of pentlandite. Abstracts, 29th International Geological Congress, vol. 3, 676 p. Kyoto, Japan.

Sugaki, A., Kitakaze, A., and Hayashi, T. (1982) High-temperature phase of pentlandite. Abstracts, Annual Meeting of the Mineralogical Society of Japan, 22 p. (in Japanese).

———(1984) The solid solution of pentlandite and its phase relations at temperatures from 600 to 800 °C (abst.). Journal of the Japanese Association of Mineralogists, Petrologists and Economic Geologists, 79, 175–176 (in Japanese).

Manuscript received July 8, 1996
Manuscript accepted August 25, 1997

Exhibit E

Infinite linear chains of Sb atoms in the novel metal-rich polyantimonides $Zr_{7.5}V_{5.5}Sb_{10}$ and $Zr_{6.5}V_{6.5}Sb_{10}$

Holger Kleinke*

FB Chemie, Philipps-Universität Marburg, D-35032 Marburg, Germany. E-mail: kleinke@mailer.uni-marburg.de

The structures of the title compounds exhibit short Sb–Sb bonds besides a multitude of bonding M–M interactions, *i.e.* the M atoms (Zr and V) in low valent states.

Partial electron transfer from the anionic to the cationic component has been used for a variety of so-called '*chimie-douce*' reactions.[1] Whereas the distances between the tellurium atoms decrease in the structures of the ditellurides from $ZrTe_2$ to $PdTe_2$ with increasing electronegativity of the metal atoms, the systematics of the Sb–Sb distances of the monoantimonides is less clear.

No Sb–Sb contacts < 350 pm occur in the structures of many monoantimonides of valence-electron poor transition metals like ScSb[2] and YSb[3] (both NaCl type), TiSb,[4] VSb[5] and NbSb[6] (all NiAs type). This may be considered as a hint to completely reduced Sb(-III). On the other hand, the structure of ZrSb[7] consists in part of puckered layers containing Sb_6 units with Sb–Sb distances of *ca.* 325 pm, which point to weak bonding interactions. This was the motivation to study Zr-rich antimonides. Here, the most metal-rich polyantimonides are presented, whose structures exhibit Sb–Sb bonds besides bonding metal–metal interactions. This observation is in contrast to related metal-rich tellurides[8] and arsenides[9] where neither Te–Te nor As–As bonds were found.

The isostructural pnictides $Zr_{7.5}V_{5.5}Sb_{10}$ and $Zr_{6.5}V_{6.5}Sb_{10}$[10] were synthesized by arc-melting of stoichiometric cold-pressed mixtures of Zr, V, and previously prepared $ZrSb_2$.[11] The metal sites are in part statistically mixed occupied by Zr and V in different ratios. The configurational entropy provides a significant contribution to the stability of these phases, which decompose during annealing at lower temperatures, namely at 900 and 1100 °C. The metal sites may be devided into two classes: the seven independent sites of the first class (white circles in Fig. 1) consist mainly of Zr atoms and form alternating triangles and rectangles parallel to the *b* axis. Five of these positions are surrounded by seven Sb atoms forming distorted pentagonal bipyramides, whereas the other two are located in pentagonal Sb_6 pyramides. The three independent positions of the second class (black circles in Fig. 1, mainly V atoms) are situated in distorted Sb_6 octahedra and Sb_5 square prisms, respectively.

Considering to a first approximation the sites of the first class solely as Zr sites and those of the second class as V sites, corresponding to a hypothetical '$Zr_7V_6Sb_{10}$', the Zr/V ratio per metal site decreases with increasing total M–Sb Pauling bond order, calculated with r_{Zr} = 145 pm, r_V = 122 pm.[12] It is concluded that the site preferences of Zr and V are mainly dominated by the different radii of the M atoms rather than by the different number of valence electrons which should influence basically only the metal–metal interactions.[13] Given the fact that $Zr_{7.7}V_{5.3}Sb_{10}$ and $Zr_{6.5}V_{6.5}Sb_{10}$ crystallize in a new structure type in addition to the occurrence of differential fractional site occupancies, these phases may be classified as typical DFSO stabilized materials,[14] being the first with the very different metal atoms, Zr and V. However, only three ($Zr_{6.5}V_{6.5}Sb_{10}$) or four ($Zr_{7.5}V_{5.5}Sb_{10}$) of the ten M sites show mixed Zr/V occupancies. On the other hand, complete ordering of the Zr and V atoms is observed in the structure of $Zr_2V_6Sb_9$.[15]

The metal atoms are interconnected *via* short metal–metal bonds with lengths between 260 and 310 pm. The majority of these interactions are found between atoms of class II parallel to [010] and between the atoms of the classes I and II, whereas only one of these relatively short bonds connects two atoms of class I, being situated in the *ac* plane [thick line in Fig. 2(a)]. The atoms of the first class form channels which include linear chains of Sb atoms with short alternating Sb–Sb distances of 280 and 288 pm for $Zr_{7.5}V_{5.5}Sb_{10}$ ($Zr_{6.5}V_{6.5}Sb_{10}$: 281 and 288 pm). It is interesting that the surrounding electropositive Zr

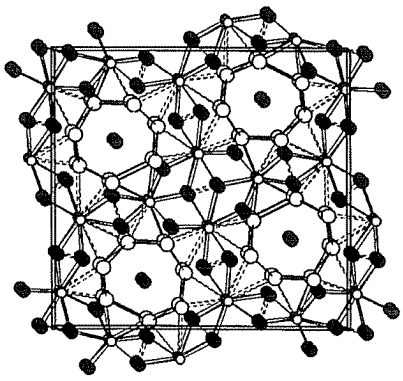

Fig. 1 Projection of the structure of $Zr_{7.5}V_{5.5}Sb_{10}$ along [010]. Large white circles: M atoms of class I (mainly Zr); small white: M atoms of class II (mainly V); medium black: Sb.

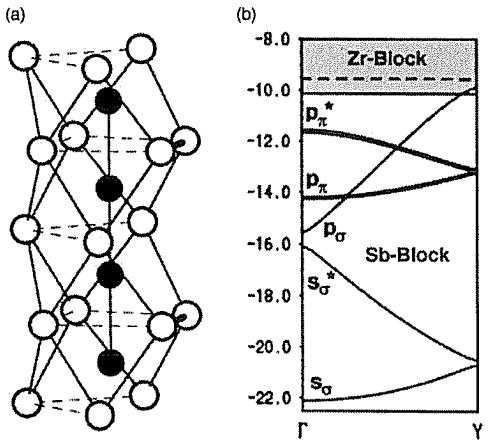

Fig. 2 (a) Part of the infinite (Zr, V)$_7$Sb$_2$ chain. Thick solid line between M atoms: distance d = 305 pm, thinner lines: 350 pm < d < 370 pm; dashed lines: 380 pm < d < 430 pm. (b) Schematic band structure of an infinite Zr_7Sb_2 unit.

atoms use some electrons for Zr–Zr bonds instead of reducing antimony to Sb(-III). Other Sb–Sb distances in this structure range from 330 to 350 pm (dashed lines in Fig. 1) which is comparable to the second shortest Sb–Sb bonds in elemental antimony (336 pm). Whereas the bonding character of these interactions remains questionable, the shorter distances, being shorter than in elemental antimony (291 pm), may be compared to the lengths of two-electron–two-center bonds found in other polyantimonides, namely in KSb (283 and 285 pm),[16] cyclo-Sb_5^{5-} (between 281 and 291 pm),[17] and Sb_{11}^{3-} (between 276 and 285 pm).[18]

However, the linearity of the Sb chain stands against two-electron–two-center bonds, as can be derived from a comparison with the zigzag Sb(-I) chains in KSb or the Te chains in elemental tellurium. In order to obtain more information about bonding in the Sb chain, the band structure of an infinite Zr_7Sb_2 chain with the atomic positions of the structure of $Zr_{7.5}V_{5.5}Sb_{10}$ (Fig. 2) was calculated using an extended Hückel approximation[19] with parameters listed previously.[15] As a consequence of the Peierls distortion, a gap occurs between the highly disperse p_σ and the p_σ* band of the Sb atoms. With the exception of the p_σ* band, all p states of the Sb atoms are located well below the Zr centered states [Fig. 2(b)]. Since the Zr states are partially occupied because of the bonding Zr–Zr interactions, seven bands of the two Sb atoms of the unit are completely filled, *i.e.* with two electrons per band. This leads to a formal consideration of these Sb atoms being Sb^{2-} which form (delocalized) one-electron–two-center Sb–Sb σ bonds. The latter gives a straightforward explanation for the linearity of the $^1_\infty[Sb^{2-}]$ chain, but not for the short bond lengths. The shortness of the Sb–Sb bonds is most likely a consequence of matrix effects, enabling a relatively short *b* axis and thus strong bonding metal–metal interactions parallel to the *b* axis. In a crude approximation, the formal electron counting schemes (ignoring the Sb–Sb interactions >330 pm) of $(Zr^{4+})_{7.5}(V^{5+})_{5.5}(Sb^{2-})_2(Sb^{3-})_8(e^-)_{29.5}$ and $(Zr^{4+})_{6.5}(V^{5+})_{6.5}(Sb^{2-})_2(Sb^{3-})_8(e^-)_{30.5}$ show a multitude of electrons (*ca.* 2.3 per M atom) being available for (delocalized) M–M bonds and result in a reasonable averaged oxidation state of −2.8 for the Sb atoms.

This work was financially supported by the Bundesministerium für Bildung, Wissenschaft, Forschung und Technologie, the Deutsche Forschungsgemeinschaft, and the Fonds der Chemischen Industrie. I am grateful to Professor Dr B. Harbrecht for his interest and support.

Notes and References

1 J.-M. Rouxel, *Chem. Eur. J.*, 1996, **2**, 1053.
2 L. H. Brixner, *J. Inorg. Nucl. Chem.*, 1960, **15**, 199.
3 B. Frick, J. Schoenes, F. Hulliger and O. Vogt, *Solid State Commun.*, 1984, **49**, 1133.
4 H. Nowotny and J. Peal, *Monatsh. Chem.*, 1951, **82**, 336.
5 J. Bouwma, C. F. van Bruggen and C. Haas, *J. Solid State Chem.*, 1973, **7**, 255.
6 L. F. Myzenkova, V. V. Baron and Y. M. Savitsky, *Russ. Metall. (transl. Izvest. Akad. Nauk SSR, Met.)*, 1966, **2**, 89.
7 E. Garcia and J. D. Corbett, *J. Solid State Chem.*, 1988, **73**, 452.
8 R. L. Abdon and T. Hughbanks, *J. Am. Chem. Soc.*, 1995, **117**, 10035.
9 H. Kleinke and H. F. Franzen, *J. Alloys Compd.*, 1998, **266**, 139.
10 *Crystal data* (IPDS, Stoe, T = 293 K): $Zr_{7.5}V_{5.5}Sb_{10}$: M = 2182 orthorhombic, space group *Pnma*; a = 1871.6(2), b = 567.22(6), c = 1764.9(2) pm; Z = 4, μ = 20.7 mm^{-1}, 2681 independent reflections; $R(F)$ = 0.036, $R_w(F^2)$ = 0.074 for 1069 observed reflections [$I > 2\sigma(I)$]. $Zr_{6.5}V_{6.5}Sb_{10}$: M = 2142 orthorhombic, space group *Pnma*, a = 1866.7(3), b = 569.09(7), c = 1753.7(2) pm, Z = 4, μ = 20.7 mm^{-1}, 2433 independent reflections; $R(F)$ = 0.060, $R_w(F^2)$ = 0.111 for 575 observed reflections [$I > 2\sigma(I)$]. CCDC 182/1007.
11 D. Eberle and K. Schubert, *Z. Metallk.*, 1968, **59**, 306.
12 L. Pauling, *The Nature of the Chemical Bond*, Cornell University Press, Ithaca, NY, 3rd edn., 1948.
13 H. Kleinke and H. F. Franzen, *J. Am. Chem. Soc.*, 1997, **119**, 12 824.
14 M. Köckerling and H. F. Franzen, *Croat. Chem. Acta*, 1995, **68**, 709.
15 H. Kleinke, *Eur. J. Inorg. Chem.*, 1998, **9**, 1369.
16 W. Hönle and H.-G. von Schnering, *Z. Kristallogr.*, 1981, **155**, 307.
17 N. Korber and F. Richter, *Angew. Chem.*, 1997, **109**, 1575.
18 U. Bolle and W. Tremel, *J. Chem. Soc., Chem. Commun.*, 1992, 91.
19 R. Hoffmann, *J. Chem. Phys.*, 1963, **39**, 1397; Program EHMACC, adapted for use on a PC by M. Köckerling, Gesamthochschule Duisburg, 1997.

Received in Bath, UK, 1st July 1998; 8/05410J